Cu and Pb–Zn–Ba deposits in the Great Duchy of Luxembourg: role of brines penetrating the basement and place in the post-Variscan tectonic history of Western Europe

Christian Marignac, Michel Cathelineau, Olivier Belcourt, Simon Philippo

Cu and Pb-Zn-Ba deposits in the Great Duchy of Luxembourg: role of brines penetrating the basement and place in the post-Variscan tectonic history of Western Europe

Christian Marignac[1], Michel Cathelineau[1], Olivier Belcourt[1],
Simon Philippo[2]

1- Université de Lorraine, CNRS, CREGU, GeoRessources, 54000, Nancy, France
2- Musée national d'histoire naturelle, 25, rue Münster, L-2160 Luxembourg

Corresponding author: michel.cathelineau@univ-lorraine.fr

Acknowledgements

This work has been financed by the National Museum of Natural History of Luxembourg (MNHL). Some data were acquired from samples from MNHL or collected in the field by the authors. We are grateful to Ch. Peiffert and MC Boiron for help in achieving and treating the LA-ICP-MS data and to Lise Salsi from the SCMEM for the SEM observations. This work has been carried out thanks to the access to the analytical capabilities of the GeoRessources laboratory (Université de Lorraine, CNRS, CREGU), in particular types of equipment financed by the CPER programme (national funds-Lorraine Region-FEDER), and Labex Ressources 21 (supported by the French National Research Agency through the national program 'Investissements d'avenir' with reference ANR-10-LABX-21—LABEX RESSOURCES 21). Dr Fusswinkel and an anonymous reviewer are warmly thanked for their detailed suggestions and comments which greatly helped to improve the manuscript.

Conflicts of interest

All authors declare that they have no conflicts of interest.

Abstract

The Great Duchy of Luxembourg comprises a Variscan basement, part of the Ardennes-Rhenish fold-and-thrust belt and an unconformable Mesozoic sedimentary cover representative of the eastern margin of the Paris Basin. The basement hosts several vein-type ore deposits, which remain almosundocumented until now, except for a few geological and mineralogical descriptions. The Stolzembourg Cu-deposit and the Martelange and Soleuvre Pb-Zn-Ba deposits occur at the boundary of several ore deposit provinces in Belgium and Germany. By coupling the mineralogy of fracture infillings and P-T-X reconstruction thanks to a detailed fluid inclusion study, the primary fluid events and associated metal transfer and deposition are described and compared with other Mesozoic deposits in the nearby areas. At Stolzembourg copper-only deposit, the anisothermal mixing between two highly saline (a Ca-Na and a Na-only rich end-member) fluids of ca.27 wt % eq NaCl and low-salinity water resulted in the chalcopyrite-Fe-dolomite deposition. The process occurred at temperatures ranging from c. 160°C to c.140°C under hydrostatic conditions at a depth of around 3 km. By contrast, the quartz preceding and following copper deposition recorded a circulation of lower-temperature brines. The copper fluid event was thus related to a transient heat advection and brine convection. Such an event is likely the Mid-Cretaceous thermal event detected at the scale of Western Europe in response to the coeval openings of the Biscaye Bay (to the west) and Valaisan (to the east) oceanic tracts. This event occurred between 130 and 100 Ma and is synchronous with a series of ore deposits in Western Europe.

Similar to the Ardennes Pb-Zn deposits, the small Pb-Zn showings would probably have been formed simultaneously in the same conditions. The Hercynian basement in Luxembourg follows a similar history to other West-European Variscan massifs after peneplaination, particularly the penetration of brines, probably in part issued from Trias formations, during a series of stages linked to major Mesozoic geodynamic events.

Keywords

fluid inclusion; Luxembourg; Ardennes Rhenish Massif; hydrothermal Cu-Pb-Zn ore deposits; brines

Introduction

In recent years, a great deal of research work was performed on the ore deposits of the Ardennes-Rhenish Massif (Rheinisches Schiefergebirge), or the Vosges-Black Forest massifs (Fig. 1). Most of these deposits are considered Mississippi Valley-type deposits formed during the Mesozoic era and to a lesser extent in the Eocene-Miocene. Numerous mineralogical, fluid inclusion and isotope data are available (e.g., Dejonghe 1998; Götte and Richter 2003; Baatartsogt et al. 2007; Pfaff et al. 2010; Staude et al. 2011, 2012a; Kirnbauer et al. 2012; Fusswinkel et al. 2013; Walter et al. 2016, 2018b, 2020; Scharrer et al. 2021). The emerging picture is hydrothermal deposits that formed close to the basement-cover boundary due to repeated mixing events between surficial waters and deeper-sited calcic brines from the Jurassic to the Miocene, as documented in the French Massif Central to the west (Cathelineau et al. 2012).

Until now, however, the hydrothermal vein-type ore deposits and occurrences of the Grand Duchy of Luxembourg at the southeastern edge of the Ardennes-Rhenish massif (Fig. 1) remained undocumented, except from a geological and mineralogical point of view in a few cases (Philippo and Hanson 2007; Philippo and Krontz 2007; Philippo et al. 2007; Philippo and Hatert 2018). A few microthermometric results were obtained by Staudt (1977) for both quartz and dolomite, but unfortunately, without precise identification of their place in the paragenetic sequence.

These ore deposits are i) the Pb-Zn occurrences of Allerborn (Longvilly) and Martelange, which are part of the "Pb-Zn district of the Ardennes" as defined by Dejonghe (1998), ii) some small barite veins (Bivels, Soleuvre), similar to their counterpart in the Black Forest, and iii) the relatively uncommon Stolzembourg dominant copper deposit. The Stolzembourg deposit has only minor equivalents in some Black Forest districts, such as Wiesloch (Pfaff et al. 2010) or the Stavelot Massif in the Ardennes massif (Hatert 2005). Further comparison is nevertheless, up to now, hindered by a lack of data on the P-T-X conditions of ore formation.

In this paper we intend to get these data and on this basis, to place the Luxembourg deposits in the timing and geodynamic context of the Mesozoic and Tertiary ore deposition in Western Europe. Representative samples of Luxembourg deposits and occurrences were thus selected for a fluid inclusion study and comparisons of fluid chemistry and P-T conditions of fluid circulation with neighbouring areas.

Geological setting

In the Great Duchy of Luxembourg, the Variscan basement is partially covered by an unconformable Mesozoic sedimentary cover. The basement is part of the Ardennes-Rhenish Massif fold-and-thrust belt and mainly outcrops in the northern part of the Duchy (Eisleck). The Mesozoic cover, in the south (Guttland), is representative of the eastern edge of the Paris Basin, with, however, a small inlier of the Hunsrück Slate outcropping in the very southeastern corner of the Duchy (Schengen) (Fig. 1).

The Luxembourg basement (Konrad and Wachsmut 1973; Bornain 2003; Roth 2003) consists of Lower Devonian (Pragian-Emsian) siliciclastic metasedimentary rocks deposited in a rift formed onto the Baltica passive margin. Several thousand meters of turbidites accumulated, with a maximum in a trough presently represented by the Eifel synclinorium and its western prolongation in the High-Ardennes Slate Belt (including Eisleck), hereafter denominated as HASB. There, 6000 to 8000 m of siliciclastic sedimentary rocks ($\leq$ 4000 m of Siegenian and $\leq$ 4000 m of Emsian) were deposited before the Late Devonian-Early Carboniferous carbonates and turbidites. They are only found nowadays on the northern limb of the Ardennes-Rhenish Massif. Peak metamorphic conditions (500°C, 400 Mpa) were attained during deep burial under extensional conditions at the end of the Devonian (Fielitz and Mansuy 1999). Starting in the Namurian (Asturian phase), the inversion of the rift led to the formation of a Variscan fold-and-thrust belt, with a main frontal thrust (the Midi-Aachen fault) and several secondary thrusts, such as the Siegen (Fig. 1). As everywhere in the Variscan belt, post-orogenic extensional tectonic conditions immediately succeeded, at c 270 Ma in the Rhenish Massif (Nierhoff et al. 2011). According to Izart et al. (2016), in the nearby Lorraine coal basin, the basement exhumation occurred in three stages, each marked by significant erosion, at the beginning of the Stephanian, in the Late Permian and the Triassic.

The unconformable cover, as observed in the Luxembourg basin, comprises a thick sequence of the classical Buntsandstein red beds (~ 170 m), Muschelkalk marls (with gypsum) and carbonates (~ 180 m), Keuper marls and gypsum (~ 230 m) suite, followed by a thick Liasic pile (~ 650 m) of marls with intercalations of sandstones (~100 m of Hettangian "Grès du Luxembourg", at the basis) and bituminous black shales (~ 150 m of Toarcian, at the top). The remnant of the pile is made by the ca. 180 m thick Dogger carbonates with formerly mined oolithic ironstones. The thickness of this cover, estimated at around 1.4 km, is a minimum owing to the Tertiary erosion. Indeed, Late Jurassic and possibly Early Cretaceous sedimentary rocks were probably present. A past study of a petroleum drill hole in the Metz area, south of Luxembourg, has revealed that the burial depth of the Toarcian hanging wall reached 750 m at the end of the Jurassic (Tissot 1967). In Luxembourg, an additional heap of about 570 m of Late Jurassic sedimentary rocks is likely, bringing the complete sedimentary cover to about 2 km. Such a thickness is comparable to the 1.9 km one estimated for

the Permian -Jurassic cover of the Black Forest (Staude et al. 2012 b). Moreover, in the nearby Lorraine basin, Izart et al. (2016) document erosion of the Upper Jurassic rocks in two Early Cretaceous erosion steps during Late Berriasian and Late Aptian. The Ardennes-Rhenish Massif area was still a source of clastic sedimentary rocks for the nearby basins at the end of the Trias (Durand 2014) and the beginning of the Lias (Thierry et al. 2014). Then, marine platform sedimentation (mainly carbonates) took place from the Toarcian to the end of the Malm. The exposure of the Tithonian-Berriasian boundary would explain the lack of more recent formations (Thierry et al. 2014). According to Stollhofen et al. (2008), a Muschelkalk cover would, however, have been present between the Brabant Massif (to the west) and the Rhenan Massif (to the east) in an N-S corridor, including our study area. Kirnbauer et al. (2012) state, "the thermo-chronological data suggest that large parts of the Rhenish Massif were covered by Triassic sedimentary rocks". Indeed, given the proximity to the present-day Mesozoic cover, it seems inescapable that Triassic and Jurassic sedimentary rocks were laid onto the Eisleck basement. Nevertheless, even admitting that the subsidence rate in the Ardennes-Rhenish Massif was similar to the nearby Luxembourg basin during the Middle-Late Jurassic, a thickness of 1 km seems the maximum possible. In the same way, according to apatite fission-track data (Karg et al. 2005), only several 100 m of sedimentary rocks covered the eastern Rhenish Massif. There, erosion of the Mesozoic cover did not occur before the Tertiary, beginning in the latest Oligocene (Ziegler and Dèzes 2007) and being achieved in the Burdigalian (Hautmann and Lippolt 2000; Kirnbauer et al. 2012).

Luxembourg copper- deposits and lead-zinc-barite occurrences

The Stolzembourg copper deposit

The Cu-bearing veins occur within the Stolzembourg Early Emsian schists as infillings of N150-170°E fractures roughly perpendicular to the synschistose hecto- to decametric folds (Philippo et al. 2007*)*. Although earlier workers thought there were up to seven distinct veins in the vicinity of the Stolzembourg mine, careful recent mapping and geophysical exploration suggest that there is only one vein, dilacerated by a series of ENE-WSW striking normal faults with a ~ 40° N dip (Philippo et al. 2007*)*.

The Stolzembourg mine was active from 1717 to 1944, and, from the few production data at hand, more than 250 t Cu were extracted. Antun (1968) states that copper-bearing wastes contain gold (8 $g.t^{-1}$Au). Gold, however, could not be observed in the studied samples.

From old mine documents, the copper was mainly contained in subvertical and more or less interconnected ore shoots in a mineralised NNW-trending fault dipping 60° to 65° to the W, which

is thought to have a dextral component. Within the ore-shoots, several 10 cm-sized vein-like chalcopyrite masses (up to 40-50 cm thick) are embedded in a dolomite (so-called "ankerite") matrix. The grades may reach 14 to 20 wt % Cu (up to 25%, and even 30% in the 18th and 19th centuries) (Antun 1968, Philippo et al. 2007). In contrast, in the intervening areas, only mm to cm-size pods of chalcopyrite are seen within the "ankerite", forming a disseminated ore grading around 2.2 wt % Cu. This ore is called "red ore" due to the thin coatings of hematite associated with quartz and "ankerite". Only the ore-shoots were mined, and the remaining disseminated ore is thought to represent a significant resource of more than 100 kt Cu, according to the speculations of Antun (1968).

The lead–zinc-barite occurrences

A few uneconomic Zn-Pb vein-type occurrences occur in Luxembourg (Allerborn, Longvilly, Martelange (Fig. 1). They are part of a small district hosted in the Lower Devonian of the High-Ardennes Slate Belt, so-called the Pb-Zn district of the Ardennes (Dejonghe 1998), except for the Soleuvre deposit, which is hosted in the Bajocian cover. In Belgium, the richest veins are located in the low-grade domains of the belt (Rocheux-Oneux: 36.5 kt Zn and 27.7 kt Pb) (Dejonghe 1998).

Materials and methods

Samples

Around thirteen samples come partly from the Luxembourg Museum of Natural History (LMNH) collections but also from new sampling, including nine samples from the Stolzembourg copper deposit (old addit), three samples from the Allerborn and Martelange Pb-Zn deposit (tailings), and one barite from Soleuvre quarry.

Micro-XRF mapping

A Bruker-Nano M4 Tornado instrument was used to get chemical maps at the sample scale. This system has an Rh X-ray tube with a Be side window and polycapillary optics giving an X-ray beam with a diameter of 25-30 µm on the sample. The X-ray tube was operated at 50 kV and 200 µA and a 2 kPa vacuum. X-ray fluorescence was detected by a 30 mm^2 xflash® SDD with an energy resolution of <135 eV at 250,000 cps. Main elements such as Si, Ca, Fe, S, Cu and Ba were mapped, and composite chemical images were generated.

Scanning Electron microscopy

After petrographic examination of the thin sections, an SEM study was conducted using a JEOL FEG7600 apparatus 7600F (hot cathode) equipped with an Oxford Instruments SDD-type EDS spectrometer to get BSE images and major element EDS analysis for the Stolzembourg dolomite.

ICP-MS

Rare Earth Element (REE) contents of dolomite were determined using laser ablation inductively coupled plasma mass spectrometry (LA-ICPMS) at the GeoRessources laboratory. Fourteen REEs (La, Ce, Pr, Nd, Sm, Eu, Gd, Tb, Dy, Ho, Er, Tm, Yb and Lu) were analysed for each experiment. All data were acquired as raw counts (cps) using the time-resolved mode. For each analysis (external standard and unknown sample), the background was measured before ablation for 20 s, and its return to its initial value was checked before ablating a new zone. Signal intensity integration of 14 REE masses was carried out during the plateau regime. Signal acquisition of the sample was stopped after 150 pulses (30 s at 5 Hz). The spot size was 60 µm, and the acquisition time was 80 s, including 20 s background acquisition and 30 s ablation. Reference materials are the certified glass standards NIST610 and NIST612 (Pearce et al., 1997). As determined by SEM-EDS, we used Mg as an internal standard (Mg). Data reduction was carried out following the standard methods of Longerich et al. (1996).

Microthermometry

Doubly polished thick sections (100 µm) were produced from representative samples across a cross-section through the central Stolzenbourg vein following the paragenetic sequence to determine the chronological sequence of fluid inclusion assemblages (FIA; Goldstein and Reynolds,1994) by optical microscopy. Fluid inclusions (FI) could be studied in dolomite and quartz by microthermometry using a Linkam THSMG600 heating-freezing stage and an Olympus BX51 optical microscope with a magnification of up to x800 (objective x80, ocular x10). The accuracy and precision of the measurements were assured by repetitive calibration of the stage. Calibration was made using nearly pure CO_2 natural FI ($_{Tm\ CO2}$ at -56.6°C, using Camperio quartz, Switzerland) and synthetic aqueous FI of known ice melting temperatures ($T_{m\ ice}$ at -21.2°C and 0.0°C). The accuracy is around ± 0.2°C for the low-temperature measurements. At high temperatures, the heating rate was 5° to 10°C.min^{-1} up to temperatures close to T_h and then reduced to 2°C.min^{-1}, yielding an accuracy of around ± 1°C. As inclusions in calcite and sulphates quickly leak, severe precautions are needed (Ulrich and Bodnar, 1988) and were taken in the present work: (i) low-temperature glue was used to impregnate the samples before polishing, (ii) the largest inclusions were avoided, (iii) the inclusions were continuously monitored during the heating, to recognise

leakage or stretching, and (iv) freezing experiments were systematically conducted after heating, as "freeze-stretching" is possible. Also, T_h measurements were iterated for each inclusion and rejected if not reproduced at ± 2°C. Bulk salinity and the presence of volatile species were checked using micro-Raman analysis performed on a DILOR LABRAM Raman spectrometer at the GeoRessources laboratory (Nancy, France).

Results

Stolzembourg

Field observations

Accessible galleries still allow observing the dolomite-"ankerite" vein system. The carbonates fill en-echelon tension joints or veins, indicating a normal faulting component (Fig. 2a, b). Matrix-supported breccias (hydraulic fracturing) are also present, usually parallel to the veins. The main veins run in the N160°-170° E60°-70°E direction, and local observation of oblique striation at the fault walls yields a dextral-normal behaviour, as already stated by Mosar (1992).

In exploration workings (Fléssen and Riedgerbësch galleries), the copper vein is associated with a parallel barite vein. A barite vein, without associated copper mineralisation, is known at the close vicinity of Bivels. There, outcropping veins of the barite system observed along with a road cut [CR355, GPS coordinates: 81894-113208] display an organisation similar to that at Stolzembourg, with the main veins running at N170°E and being offset by pull-apart jogs along the N10°-20°E direction, indicative of a dextral-normal setting.

Observations at the sample scale

At the outcrop and sample scales, both brecciation and repetitive fracture opening and filling are observed (Fig. 2, 3 and 4). Vein filling starts with quartz, typically featuring a comb texture (Fig. 4c), followed by thick dolomite. Late quartz (locally known as "diamond quartz") occupied incompletely filled, open vugs (Fig. 3b, c).

Breccias may either occupy the whole vein or, in the ore shoots, are located in the vein wall rock. All breccias are matrix-supported, typical of hydraulic fracturing. The clasts are fragments of the wallrocks, varying in size from a few cm to a few mm, typically reddened (Fig. 3b, 4a). Wallrocks are typically reddened on distances ranging from several centimetres to metres from the boundary. Clasts featuring the reddening border are present in the breccias (Fig. 4a), indicating that the reddening preceded the brecciation.

The breccia matrix is formed either by coarse-grained dolomite (Fig. 3b, 4a) or by fine-grained quartz aggregates reddened by association with hematite ("red ore") (Fig. 3a).

Chalcopyrite is later than dolomite (Fig. 3c, f), which may have been dilacerated (Fig. 4b).

Although not observed in present-day accessible galleries, barite was observed in some samples from the LMNH collections, where barite appears earlier than the quartz-ferroan dolomite association (Fig. 4d).

Paragenetic succession

A synthetic paragenetic succession may be constructed by combining sample-scale and microscopic observations, excluding supergene associations. Three stages are distinguished (Fig. 5): a first stage corresponding to the emplacement of the dolomite veins, a main mineralising stage with chalcopyrite deposition, and a late stage marked by euhedral quartz deposition (so-called "diamond quartz"). The expression of the different stages varies from one vein to the other: dolomite is the dominant mineral of the early stage in the Stolzembourg vein, while it is quartz in the Riedgerbësch occurrence.

The early stage consists of quartz (Q1 and Q2) and saddle dolomite (Dol1). The first quartz generation (Q1) occurs as microcrystalline quartz in the breccia matrix. It currently contains fine-grained hematite (Hm1) and relicts of tiny barite prisms (Fig. 6a), containing up to 5.6 wt % Sr. Uncommon, small (≤ 1 μm) inclusions in Q1 are found by EDS to be mainly composed of Cl, C and Pb, with minor As and Cu, suggesting that the included mineral is phosgenite $Pb_2(CO_3)Cl_2$. Q2 quartz is euhedral and forms overgrowth on Q1 aggregates but comb ribbons at the vein selvages (Fig. 4c). Dolomite Dol1 (Fig. 7a) usually crystallises onto Q2 quartz but may be directly overprinting Q1. Pyrite1 preceded the dolomite and occurred at the Q2-Dol1 boundary. A unique observation shows a complicated history, with a pyrite "nodule" filled with skeletal barite, Dol1 and pyrite. Most pyrite, however, is found as euhedral crystals within chalcopyrite and could, therefore, be related to the main ore stage, being a pyrite2. Dolomite Dol1 is saddle dolomite, commonly exhibiting a plumose texture (Fig. 7b-d). Dol1 is locally internally complex, displaying irregular zoning patterns under SEM and μ-XRF examination (Fig. 6d). Zoning is caused by slight variations of the Fe content with compositions varying from $CaMg_{0.6}Fe_{0.3}Mn_{0.1}(CO_3)_2$ to $CaMg_{0.5}Fe_{0.4}Mn_{0.1}(CO_3)_2$. As already noted by Philippo et al. (2007), these compositions lie indeed outside the ankerite field. However, the saddle crystals of Stolzembourg were called "ankerite" for a long time by successive collectors. According to Philippo et al. (2007), other carbonates (calcite, siderite) may also be found at Stolzembourg, but their paragenetic position remains obscure.

The main mineralisation stage followed a renewal of tectonic opening, marked by the second generation of comb ribbon quartz (Q3), preceding the chalcopyrite deposition in the quartz-rich portions of the system (Fig. 4c, 6c). The second generation of dolomite (Dol2) is observed, commonly as mm-size overgrowths on Dol1, and also as small euhedral Dol2 crystals (down to 20-30 μm) incorporated into chalcopyrite and found under SEM examination to contain tiny hematite

prisms (Hm2, up to 1-5 µm). Dol2 dolomite is ferroan, although less than Dol1, with a composition $CaMg_{0.7}Fe_{0.3}(CO_3)_2$ practically devoid of manganese. Philippo et al. (2007) state that rare cubanite, sporadic galena, and sphalerite are associated with chalcopyrite.

The *late stage* is represented by the "diamond quartz" Q4 (Fig. 4c, 7e-f), which displays growth zoning with internal plumose textures (Fig. 7f). Q3 may be absent, and chalcopyrite expression is highly reduced, and in such cases, Q4 seems to lie directly on the Dol2 dolomite (Fig. 6e-f).

REE profile of Stolzembourg dolomite

All generations of Stolzembourg dolomite display identical chondrite-normalised REE distribution patterns with a typical bell-like disposition (Fig. 8). Such MREE-enriched patterns are rarely encountered in hydrothermal carbonates, except in a few instances, such as the dolomite from U-deposits found around unconformities in Saskatchewan, Canada (Richard et al., 2010). A few similar MREE-enriched patterns are presented in Fig. 8, A, some for ankerite from the nearby Black Forest deposits (Staude et al. 2012a), others more exotic: siderite from cold methane seeps in the Niger delta (Rongemaille et al. 2011) and calcite from a Carlin-type gold deposit in China (Shuiyidong: Su et al. 2009), the latter being by far the closest to the Stolzembourg carbonates.

Fluid inclusions study

FI petrography: Fluid inclusion assemblages (FIAs) for all petrographic types were interpreted and classified according to their relative age in the paragenetic sequence. FIs are abundant in dolomite (Dol1, Dol2) and are primary, as they distribute along crystal growth zones. Studiable FIAs follow some dolomite growth bands, as shown in Fig. 9a, where they are particularly abundant; the last growth band of Dol2 is generally devoid of FI (Fig. 9a). In the growth zone, FIs are grouped as clusters (Fig. 9b). Their morphology is elongated, frequently parallelipedic and their distribution in dolomite is geometrically controlled by the geometry of the crystal with Fi edges parallel to the growing face and cleavage (Fig. 9 c and d). FIs are scarce in quartz except in localized clusters of primary inclusions (Q2, Q4) in some growth zones, as shown in Fig. 9 e. Q1 was not studied as too microcrystalline. FIs exhibit irregular and angular shapes, as shown in Fig. 9 f; some small-size healed cracks can be considered pseudo-secondary as they are not transgranular. No evidence of boiling was observed in the investigated samples.

As almost all FIs are primary, the relative chronology of the fluid inclusions follows the succession of the paragenetic sequence: quartz 2, dolomite (mostly II) characterized by large crystals, and euhedral quartz Q4.

341 *Microthermometry*: Most FIs are small (≤ 10 µm), thus making difficult the observation of ice
342 melting in dolomite. A few ice melting measurements were, however, possible. When observed, the
343 first apparent melting temperature of ice (T_e) is usually low and close to or lower than -40°C,
344 indicating the presence of divalent cations in the fluid compositions. In such a case, observing
345 hydrohalite and ice melting behaviour is a prerequisite for interpretation in the $CaCl_2$-NaCl-H_2O
346 model system (Bodnar 2003). Hydrohalite was the first to melt at a temperature comprised between
347 -35° and -25°C when its observation was possible. Ice melting ranges from -13 to -24°C in quartz
348 and from -11 to -28°C in dolomite (Fig. 10 and 11, Table 1). All the FI are 2-phase, and bulk
349 homogenisation is in the liquid phase. For a given sample, results are usually very homogeneous.
350 Based on $T_{m\ ice}$ measurements, salinity is high (Fig. 10), and the T_h range from 100° to 150°C (Fig.
351 11).
352 *Fluid composition and evolution:* Based on the hydrohalite melting temperatures, the
353 $CaCl_2$/($CaCl_2$+NaCl) ratio estimated in the H_2O-$CaCl_2$-NaCl model system (Bodnar 2003) ranges
354 from 0.49 and 0.86. The Stolzembourg fluids are, therefore, highly calcic brines (Fig. 10). Using
355 the Na/ Ca ratio, the bulk salinity was estimated from the ice melting temperature using diagrams
356 from Steele-MacInnis et al. (2011) and ranges from 15.1 to 25.0 wt% eq ($CaCl_2$+NaCl). Raman
357 spectrometry using the H_2O band (Dubessy et al. 2002) confirmed the validity of this chlorinity
358 range. Thus, on the sample ZA074 FIs, the chlorine content estimate issued from Raman
359 spectrometry data (3 to 3.8 mole Cl) is similar to the estimate from microthermometry (15 to 18%
360 wt eq (NaCl+$CaCl_2$)).
361 The T_h-$T_{m\ ice}$ diagram in Fig. 11 shows two distinct trends, one more characteristic of the
362 dolomite-hosted FI (trend 1) and the other of the quartz-hosted FI (trend 2). As some FI are
363 secondary, it is unsurprising that some FIs from either the dolomite or the quartz are associated with
364 opposite trends (group 2 for dolomite, group 1 for quartz). On the one hand, most of the dolomite-
365 hosted FI (comprising all the possible primary FI), while exhibiting the highest T_h (ranging between
366 130 and 150°C), display an inverse T_h-$T_{m\ ice}$ relationship. Such a trend could correspond to a more
367 or less isobaric anisothermal mixing trend. Interestingly, the data from Staudt (1977) coincide with
368 trend 1 (Fig. 11), extending the high salinity to up to 26.5 wt % eq. ($CaCl_2$+NaCl). On the other
369 hand, the quartz-hosted FIs are characterised by a more dispersed behaviour, with lower T_h in the
370 120° to 100°C range and a salinity range as in the previous trend. Salinity is, however, restricted to
371 the 17.4 and 23.2 wt % eq ($CaCl_2$+NaCl) range. This second group may consist of several more or
372 less parallel trends (trends 2, Fig. 11), thus recording isothermal fluid mixing under fluctuating
373 pressure conditions. Such an interpretation would be consistent with the textures testifying for
374 hydraulic fracturing and crack seal in quartz (see above § 4.1.2).

The lead–zinc-barite occurrences

Martelange Ba-Pb

The mineralised system is no more visible at the outcrop, but sampling is possible in the old mine wastes. The mineralisation occurs in Late Pragian slates ("ardoises"). Barite, siderite, pyrite and galena are hosted by old (late Variscan) quartz veins reworked at the mineralisation stage deemed to be Mesozoic. The Martelange samples of the same generation presented in the Luxembourg Museum only show sulphide mineralisation, dominated by pyrite: stockworks of pyrite veins (apparently formed through hydraulic fracturing) are reworked (dissolution-recrystallisation), and late cubic pyrite followed by cuboctahedral galena crystallised in the resulting vugs. A small quartz vein with barite was studied for FIs, but the only FIs found were in the quartz and appeared to be late Variscan metamorphic fluids, as shown by the density of volatile components.

Allerborn - Longvilly Pb-Zn

The Allerborn Pb-Zn showings are hosted in Variscan quartz veins in the regional NE-trending Wardin fault (Fielitz and Mansy 1999). These quartz veins are boudinaged, and primary FI are naturally decrepitated and could not be studied. When these quartz host Pb-Zn ores, secondary fluid inclusion as FIPs are present. They are very small (≤ 10 µm) 2-phase FI, with an ice melting temperature ranging between -6° and -2°C, yielding a bulk salinity of 3.4 to 9.2 wt% eq NaCl in the NaCl-H_2O model system (Bodnar 2003)). These FIs homogenise in the liquid state at temperatures between 210 and 300°C, with however two modes at ca. 230-250°C and 270-290°C, the latter suggestive of a post-trapping re-equilibration process (stretching?). The sphalerite contains a few small (< 10 µm) FI, in which no melting temperatures were observed, but only one bulk homogenisation temperature (95°C).

Soleuvre barite

Unfortunately, as is often the case in the Black Forest deposits (e.g. Staude et al. 2012a), most barite crystals in Luxembourg occurrences lack measurable FI. Only in a barite vein in the Bajocian cover at Soleuvre were some FI visible. They are small (≤ 10 µm) regular 2-phase inclusions homogenising into the liquid phase. Unfortunately, owing to both the scarcity in FI and the very brittle behaviour of barite, only one $T_{m\ ice}$ (-8.5°C) and one T_h (100°C) could be measured. Salinity estimated in the NaCl-H_2O system is ca. 11 wt % eq. NaCl.

Discussion

The Stolzembourg vein system and its relationships with the barite vein systems

Our proposed paragenetic succession is consistent with the paragenetic sequence presented, as a synthesis of earlier works and new observations, by Philippo et al. (2007), the main differences lying in our introduction of early (Q1) and late (Q4) quartz generations on the one hand, and the barite position, on the other. Barite was considered younger by all previous workers. Yet, in our copper-bearing samples from the Stolzembourg mine, the only barite we found was in the earliest Q1 quartz, where it was replaced, leaving only relicts (with up to 5.6 wt % Sr). Moreover, some samples from mineral collections at the Stolzembourg or Luxembourg museums and labelled as coming from the main copper mine, display the relationships between large euhedral barite crystals and a quartz-dolomite association (very reminiscent of the Q2-Dol1succession), with clear evidence of overprinting of the former by the latter (Fig. 4d). Also, Philippo et al. (2007) report that on the occasion of piercing a drain adit for the Our hydroelectric plant, euhedral barite crystals were collected from the Bivels barite vein, and that euhedral chalcopyrite crystals overgrew them. A stage of barite deposition thus clearly preceded the main mineralisation stage.

In the Bivels outcrops, however, barite was later than the ferroan carbonate and, therefore, than the copper episode, although associated with the same dextral-normal structural pattern. Yet, the Bivels and Stolzembourg (Fléssen and Riedgerbësch veins) barites contain some strontium, as does the earliest barite from the Stolzembourg copper ore, although in lesser quantity (3.2 wt% Sr at Bivels, 2.7% at Fléssen and 1.8% at Riedgerbësch: Philippo et al. 2007). One might be tempted to see the indication of a penecontemporaneity between these different barite occurrences, but we do not think this is very conclusive. In conclusion, although the question of the relative timing between the chalcopyrite and barite vein systems cannot be considered definitively settled, it may be tentatively proposed that the dolomite-chalcopyrite vein system at Stolzembourg was intercalated between two barite vein systems: an early one represented by the Fléssen and Riedgerbësch veins (and the remnants in the Stolzembourg Q1 quartz) and a later one represented by the Bivels system.

P-T-X evolution

Fluid compositions and evolution at Stolzembourg

The Stolzembourg fault infillings result from two events of brine circulation and mixing: a low-temperature one, mostly recorded in pre- and post-mineralisation quartz, and a higher-temperature one, recorded in saddle dolomite and, in particular, in syn-chalcopyrite Dol2 dolomite. The latter is characterised by the anisothermal mixing of a $\geq$ 150°C (higher recorded T_h), $\geq$ 27 wt eq % ($CaCl_2$+NaCl) brine L1 with a lower salinity ($\leq$ 10 wt % eq $CaCl_2$+NaCl) and slightly lower temperature ($\geq$ 130°C) aqueous fluid L2 (Fig. 11). A complication arises however when the Ca content is taken into consideration: it appears that the L1 brines display the full range of measured

Na/Ca ratios for the same bulk salinity, meaning that "L1" would indeed be itself a mixture of two brines, one (L1a) far more calcic (Na/Ca $\leq \sim 0.2$) than the other (L1b, Na/Ca $\geq \sim 1.1$) (Fig. 10). Hydrohalite melting temperature was, unfortunately, difficult to measure in lower salinity FI. Still, the few obtained data suggest that the diluting L2 fluid is close to pure water (Fig. 10).

The low-temperature brines may represent the "regional" fluid circulations during copper mineralisation. Trend 1 records the local invasion by a hotter brine, yielding to the dolomite deposition as carbonates have a retrograde solubility and, most probably, chalcopyrite deposition.

P-T conditions at Stozembourg

Isochores were constructed for representative FIs (Fig. 12). As presented above, FIs in quartz record mixing events at various pressures. As far as this may be considered as due to crack-seal processes, it may be hypothesised that this variation consisted of switches from litho- to hydrostatic pressure conditions (Fig.11). Under this assumption, it is possible to retrieve a pressure estimate at the time of quartz deposition by considering two extreme isochores, the one with the lesser slope (T_h 120°C) supposed to represent trapping under hydrostatic conditions, the steeper one (T_h 100°C) taken as representative of lithostatic conditions. With the assumption of isothermal mixing at the T_0 temperature, the two pressures obtained by the intersection of the T_0 isotherm with the lithostatic and hydrostatic isochores, P_0^L and P_0^H, respectively, must be such that $P_0^L = \rho * P_0^H$, where ρ is the mean density of the superincumbent rocks. This condition is attained by an iterative "trial-and-error" method. The method is not very sensitive to the density value, the results being very similar for ρ=2.6 and ρ=2.7 (Fig. 12): the condition is met for T_0 = 132°C and P_0^H = 28 MPa, i.e., at a depth of 2.8 km. This depth is compatible with regional estimates, such as those proposed for the southern Black Forest district: 2.5 to 3 km depth, according to Walter et al. (2015). Given that formation depth, the anisothermal but isobaric mixing between the two L1 and L2 brines involved in the dolomite-chalcopyrite cycle is seen in Fig. 12 to proceed between 162°C, or more (L1) and 142°C, or less (L2). The corresponding geothermal gradient is estimated at $\sim 48°C.km^{-1}$, pointing to an anomalous thermal regime in the Luxembourg crust at the time of copper deposition.

Nature and source of fluids in the regional context

In the Ardennes-Rhenish Massif, as well as the Vosges and the Black Forest, deposits are characterised by the circulation of brines at relatively low temperatures (FI T_h comprised between 50° and 150°C or more) (Dubois et al. 1996; Heijlen et al. 2001; Muchez et al. 2005; Baatartsogt et al. 2007; Pfaff et al. 2010; Staude et al. 2011, 2012b; Fusswinkel et al. 2013, Walter et al. 2018a) (Fig. 13). In the Black Forest, a clear-cut difference is observed between the Jurassic-Cretaceous and post-Cretaceous deposits when the brine compositions are considered: as seen in Fig. 13, the

476 former is characterised by higher salinity, and more calcic composition of the brines, compared to
477 the later (Pfaff et al. 2010, Walter et al. 2015). On this basis, Fig. 13 demonstrates that based on the
478 composition of the fluid inclusions, it would appear the Luxembourg deposits are members of the
479 Jurassic-Cretaceous family.
480 All the above-cited workers on the Black Forest or Ardennes deposits concur in admitting the
481 existence of several fluids and their mixing as a cause of ore deposition (Fig. 13).
482 The nature of these fluids is, however, discussed. In the Black Forest, post-Variscan deposits
483 resulted from the "large scale mixing of a basement-derived saline NaCl-$CaCl_2$ brine with meteoric
484 water", according to Schwinn et al. (2006), as indeed well seen in the T_h-$T_{m\ ice}$ diagram (Fig. 13).
485 The deep brine would be therefore both metal- and S-rich (likely as sulphate ions, thus raising the
486 question of the reducing agent at the locus of deposition). However, as demonstrated by Fusswinkel
487 et al. (2013) and emphasized by Walter et al. (2015), two types of brines are involved in the
488 formation of Jurassic-Cretaceous deposits: a NaCl-dominated brine and a Ca-rich brine, and this is
489 also the case for the Stolzembourg Cu deposit in Luxembourg (Fig. 10). In a detailed survey of the
490 Jurassic hydrothermal veins in the Black Forest, Walter et al. (2017) demonstrated that the brine
491 salinity and Ca/Ca+Na ratio were apparently under the dependence of the nature of the former
492 Triassic cover (halite-bearing or not). According to Staude et al. (2011), for the Black Forest
493 deposits, the two participating brines are: i) a deep one (rooted at 7 to 8 km depth), the Na-rich brine,
494 the basement brine, and ii) "stagnant formation water" the Ca-rich (Ca-Na exchanged) brine derived
495 from the cover reservoirs. The reservoir for this "formation water" component is usually considered
496 the Permo-Trias red beds from the cover: "red bed-derived fluids". According to Staude et al. (2012
497 b), although ore components may be derived from various sources, including magmatic and
498 metamorphic rocks and red-beds sedimentary rocks, the latter are "the most probable ones". Where
499 such red-beds were not deposited onto the southern Black Forest basement, the Muschelkalk
500 carbonate platform is thought to have acted as the reservoir (Walter et al. 2015). By FI microanalysis
501 of a south Black Forest vein, Fusswinkel et al. (2013) also demonstrate the mixing between a calcic
502 brine with Na/Ca ≤ two and a sodium-dominated brine. They consider that the latter, with elevated
503 Cl/Br ratios, came from halite dissolution (i.e., from a Triassic evaporite reservoir), with some Ca
504 enrichment by Na-Ca exchange reactions along the flow path through the uppermost parts of the
505 basement. In contrast, the calcic brine, with typically low Cl/Br ratios, was a bittern brine, having
506 resided in a basement reservoir. Moreover, the microanalysis concluded that the metal-rich brine
507 was the basement brine, the halite dissolution brine being, by contrast, metal-depleted but S-rich. In
508 the same way, Walter et al. (2016) conclude their regional study of the Jurassic-Cretaceous fluids
509 in the Black Forest deposits by identifying an "older" bittern, which was stocked in the basement

and suffered a long-term fluid-rock interaction (the calcic brine), and a "younger" sodic brine evolved by halite dissolution in the cover, and Walter et al. (2018a) conclude to "multi-component fluid mixing processes" implying several reservoirs.

The basement bittern brines are usually thought to come from the Mid-Triassic evaporites initially and then have penetrated deep into the basement during early Mesozoic extensional episodes. Such an origin is demonstrated in the Black Forest (Bons et al. 2014; Walter et al. 2016) or the western French Massif Central (Boiron et al. 2002; 2010; Cathelineau et al. 2012). For the Belgium Pb-Zn deposits, however, in an area where Triassic evaporites were never deposited, Dejonghe (1998), Heijlen et al. (2000), Dewaele et al. (2004) and Muchez et al. (2005) consider the late-Variscan infiltration in the deeper crust of brines derived from Carboniferous evaporites, which are well known (by drilling) in the autochthonous Visean in front of the fold-and-thrust belt. This early infilling of deep reservoirs able to be remobilised at different times is consistent with the diversity of the hydrothermal events in the considered areas, which, as underlined by Pfaff et al. (2009), supposes that "through time, the same fluid source was repeatedly involved in the formation of hydrothermal vein deposits".

The deposition mechanism may be the following succession: old bittern fluids having reached a significant depth where they resided a long time, received their calcium content, then scavenged metals, and rapidly ascended to the surface when pressure was released. There, they developed hydrofracturing and encountered younger shallow-level fluids with which they may have mixed (Staude et al. 2009; Bons et al. 2014; Walter et al. 2016). However, the residing time would be several 10 Ma (up to 100 Ma: Muchez et al. 2005). There is, in conclusion, a consensus on the participation of a "basement brine".

Such sequestration in the long term of basin-derived brines in a deep basement in relation to the development of continental crust permeability (Gleeson and Yardley 2002; Ingebritsen et al. 2010) is indeed well documented. In the Äspo Scandinavian basement, brines were trapped for more than 1.5 Ma (Louvat et al. 1999). More significantly, the residence time of the brines observed at 4 km depth and more in the KTB continental-drill hole is longer than 30 Ma (Fehn and Snyder 2005). These fluids are indeed thought to have been trapped in a deeper reservoir during the Mesozoic and remobilised to their present position in the late Cretaceous (Lodemann et al. 1998; Möller et al. 2005).

In the SE margin of the French Massif Central, Aquilina and de Dreuzy (2011) came to the conclusion that present-day fluids trapped in the micropores of the Permian reservoir (at a 634 m depth) resulted from the early to middle Jurassic (200-160 Ma) circulation of brines laterally derived from the Triassic evaporites in the subsiding SE Basin. In the same way, Boiron et al. (2002) and

Cathelineau et al. (2004) document, on the NW margin of the Aquitaine Basin, the deep penetration in the Variscan basement of brines issued from the basin at ca. 120 Ma and the sequestration of these brines in the micropores of the granites up to nowadays. Brine residence times in the basement of 50 Myr and more are equally demonstrated in the U.S. midcontinent (Thornton and Wilson 2007). A far longer sequestration time may be observed when formation brines trapped in shale aquicludes are directly dated, as the brines of the Ordovician age are presently found at 860 m depth below the Michigan Basin in Canada (Clark et al. 2013).

The two brines observed at Stolzembourg match well the "basement/cover" brine model proposed for the Black Forest deposits (Fig. 11): the two brines both represent the hot end-members of the anisothermal mixing process and, indeed, must be considered as "basement" brines, mixed on their way to the deposition locus. Still, dilution by a less saline and colder fluid is also implied (Fig. 11 and 13).

Copper transport and precipitation: the need for an oxidising fluid

Copper is transported in solution in the Cu(I) valence state, mainly as a $(CuCl_2)^-$ complex (Xiao et al. 1998; Mei et al. 2013), and is then found under the same valence state in copper sulphides (Goh et al. 2006). No redox change would thus be needed a priori for copper deposition. However, under reducing conditions and relatively low temperatures (< 250°C), copper solubility as a Cu(I) chloride complex is so low that it precludes significant copper transportation unless conditions are unusually oxidized (Xiao et al. 1998). In the Stolzembourg case, an oxidising fluid was needed to transport copper to the deposition site at temperatures between 150 and 200°C. Indeed, at Stolzembourg, the transient presence of oxidising fluids is marked by the wall-rock reddening and the hematite occurrences, including the tiny hematite in the Dol2 rhombohedra, immediately preceding the chalcopyrite. The source of the oxidising fluid could have been an Early Cretaceous regolith (see below). Reduced fluids were, however, necessary to provide iron to the locus of hematite and chalcopyrite deposition, and fluid mixing is therefore required, as observed in the fluid inclusion record.

Chalcopyrite deposition also requires the presence of reduced sulphur. Reduced sulphur could have been present in one of the involved fluids (but not the copper-bearing one!) or have resulted from sulphate reduction. In the latter case, reducing the sulphur could have been related to a TSR process producing reduced sulphur from brine sulphate ions, driven, for instance, by methane. The process demands, however, the former presence of H_2S as a catalyser (Truche et al. 2014). If the reduction had occurred near the deposition site, BSR could have fulfilled this prerequisite at the lower temperature of fluid circulation attested before the chalcopyrite event. It remains speculative in the

absence of C isotope data at Stolzembourg to prove the methane intervention. Nevertheless, in the Ardennes belt, the FI homogenisation temperatures are consistently between 110° and 150°C, and low $\delta^{13}C$ in calcite, together with most $\delta^{34}S > 10‰$ are data in favour of methane-driven TSR for the origin of the sulphur for the sulphides (in Dejonghe 1988). The source of sulphate is thought to have been the thick anhydrite beds known by drilling in the autochthonous Visean (Muchez et al., 1995). The methane could have been produced by interaction with organic matter of the deep and hot fluids, somewhere on their path from the deep reservoir, or even through their equilibrium with basement graphite, as proposed for the deepest fluids from the Black Forest by Staude et al. (2012 a). By directly observing hydrocarbons trapped in sulphides from the Pb-Zn deposits in the nearby Rhenish Massif, Jochum (2000) argues the local heating of kerogen by the hot Mesozoic basement fluids.

In general, copper deposition may be triggered by decreased temperature, fO_2 and bulk salinity, and increased pH (Xiao et al. 1998). At Stolzembourg, all these conditions were met, notably the chlorinity decrease at the time of ore deposition: the FI data indicate temperature and bulk salinity decrease. The inferred existence of reducing fluids (Fe^{2+} transportation, production of HS^-) may be taken as evidence for a lowering of fO_2. This conjunction of favourable factors might have allowed the formation of a significant deposit even if the bulk copper content of the mineralising fluids was not high. However, such conditions are not infrequently encountered in many Pb-Zn deposits and cannot explain why copper-only deposits are so scarce in the Mesozoic record of Western Europe.

Sources of metals and trace elements

Significance of REE data

At Stolzembourg, the REE pattern in the syn-ore dolomite is a possible direct insight into the source area(s). According to Rongemaille et al. (2011), there is no REE fractionation during the carbonate deposition; thus, an REE spectrum is representative of the forming fluids. On the other hand, the total REE abundance, controlled mainly by the mineral growth rate and the fluid flow rate (Möller et al. 1991), does not directly depend on the REE source. The observed pattern at Stolzembourg shows a moderate bulk REE enrichment and a strong MREE enrichment relative to both the highly depleted LREE and the HREE ("bell-shaped" or "hat-shaped") (Fig. 8). In addition, no europium anomaly is found. As seen in Fig. 8, although ankerites from the Black Forest deposits display contrasted profiles, they are in general much different from the Stolzembourg "ankerite" (some even exhibiting an inverse behaviour, as at Wittichen), with the noticeable exception of the Waldkirch ankerite (Staude et al. 2012a), which shows an MREE-enriched pattern. The Waldkirch ankerite is intergrown with chalcopyrite and is enriched in copper (up to 270 ppm Cu) (Staude et al. 2012a).

612 Compared to other ankerites from the Black Forest, it also displays an exceptionally heavy $\delta^{13}C$
613 signature, supposed to dismiss the influence of basement brines in its genesis (Staude et al. 2012a).
614 However, the reason for such a conclusion is somewhat unclear. As shown in Fig.8, several fluorites
615 of the Black Forest (Schwinn and Markl 2005) equally show MREE-enrichment, with, however,
616 less depleted HREE and, above all, LREE. At the world scale, only a few carbonate samples
617 (indifferently, ankerite, siderite or calcite) display the typical "bell-shaped" pattern of Stolzembourg
618 (Fig. 12 d). The most similar profiles are those of the mid-proterozoic Saskatchewan carbonates,
619 which also have bell-shaped REE profiles close to UO_2 profiles. These carbonates were formed by
620 mixed Na-Ca brines close to the unconformity at around 200°C (Richard et al., 2003). The calcite
621 from the Shuyindong Carlin-type deposit in China (Su et al. 2009), the siderite from the present-day
622 methane-seeps in the Niger Delta (Rongemaille et al. 2012), and, to a lesser extent, the calcite from
623 the world-class Xikuhangshan Sb deposit (Peng et al. 2003), also present bell shape profile when
624 normalized to chondrite. Unfortunately, most authors do not propose an explanation of the MREE-
625 enriched patterns. For the Black Forest fluorites, however, these patterns are interpreted as recording
626 "a basement source" (Schwinn and Markl 2005).
627 Based on a bibliographic review, Hecht et al. (1999) consider that "upward convex or roof-shaped
628 REE patterns of hydrothermal fluids seem to be typical for crustal fluids that have interacted with
629 pelitic metasedimentary rocks most probably under acid conditions". On the other hand, to explain
630 the observed MREE-enrichment of acid and hypersaline groundwaters found in arid areas of
631 Australia and Texas, Johannesson et al. (1996) invoke the preferential leaching of detrital Fe-Mn
632 oxide-hydroxides which are known to concentrate the MREE (e.g., Bayon et al. 2004; Négrel et al.
633 2006). Unfortunately, in these oxide-hydroxides, the LREE are often more concentrated than the
634 HREE, and their leaching is, therefore, unable to yield the desired "bell-shaped" pattern (which is
635 not observed in the just mentioned hypersaline groundwaters when chondrite-normalized). By acid
636 leaching of Fe hydroxides from Eifelian and Givetian siliciclastic sedimentary rocks in the
637 northeastern Rhenish Massif, Zwing et al. (2009) obtain relatively flat REE patterns, which,
638 although slightly MREE enriched, cannot, however, better match the Stolzembourg pattern (Fig. 8).
639 Finally, "bell-shaped" profiles have been observed in the solute load from the acidic Vosges rivers
640 (Tricca et al. 1999) and in experimental (acid) leachates obtained from Paleozoic anchizonal meta-
641 turbidites (Ohr et al. 1994) (Fig. 8). In both cases, the MREE-enrichment is interpreted as due to the
642 preferential leaching of apatite: it is well known that apatite concentrates the REE at an early
643 diagenetic stage (Lev et al. 1998) and that, in particular, the biogenic apatites display typical "hat-
644 shaped" REE patterns (Grandjean-Lecuyer et al. 1993). Also, dissolution experiments demonstrate
645 that apatite dissolution is far faster under acid conditions than other REE-bearing minerals, such as

monazite or florencite (Köhler et al. 2005). Moreover, these experiments demonstrate that in the first steps of the dissolution, the LREE remain sequestered in the residue due to the re-precipitation of rhabdophane (Köhler et al. 2005). As pointed out by Debruyne et al. (2016), such a retention effect is the most convenient explanation for such a highly depleted LREE pattern as observed at Stolzembourg (and in very few other occurrences, see Fig. 8d), which indeed contrasts with much of the published "bell-shaped" patterns, in which LREE are currently less depleted than the HREE (Fig. 8).

Alternatively, the REE could have been leached from a combination of phosphates and Fe-Mn oxides in a regolith. Indeed, In the kaolin clay deposits of the Rhenish Massif, Dill et al. (1995) report the presence of both LREE- and HREE-rich alumino-phosphates (florencite-goyazite and gorceixite, respectively); the clays are supposed to be Tertiary, and supergene K-Mn oxides from the southern Rhenish Massif were dated from the late Tertiary (25-1 Ma, $^{40}Ar/^{39}Ar$: Hautmann and Lippolt 2000). Such an alternative would, however, imply a Tertiary age for the Stolzembourg deposit, which is considered unlikely (see below). There is, unfortunately, no published information on the possible presence of REE-bearing minerals (other than the Fe-Mn oxy-hydroxides) in the lower Cretaceous regolith, which would otherwise be an appealing alternative. To conclude, although a contribution of the dissolution of Fe-Mn oxy-hydroxides cannot be ruled out, it seems most likely that the REE pattern of the Stolzembourg "ankerite" records the dissolution of apatite in the Lower Paleozoic turbidites from the HASB, i.e., points to sourcing of at least part of the ore-forming brines in the basement.

On the other hand, the lack of any positive europium anomaly (Fig. 8a) does not favour a Ca to Na exchange process with the feldspars in the basement to explain the Ca-enrichment of one of brines at Stolzembourg. Consequently, the Na-rich brine could have been the basement brine derived from a brine coming laterally from the Keuper evaporites in the nearby Luxembourg basin. This brine deeply infiltrated during the Early Jurassic extensional events and was sequestered until the early Cretaceous. A similar process of long-term sequestration of brines in the basement is invoked by Heijlen et al. (2003) for Silesian deposits, where Triassic brines were the pristine brines. During the same event, the calcium-rich brine could come from the locally overlying Muschelkalk cover (gypsum-bearing marls) and could have interacted with Permian red beds (see below).

5.2. Source of copper

In line with the findings of Fusswinkel et al. (2013), showing that in the Black Forest hydrothermal systems, the metal-rich brines were sourced in the basement, it may be asked if the HASB basement could have been a copper source. Although leaching of ordinary basement rocks in cataclastic zones is experimentally demonstrated to yield metals to the solution, the copper contents of minerals in

680 “ordinary” basement rocks are so low as to preclude the formation of a brine significantly enriched
681 in copper (Burisch et al. 2016). Thus a specific source is likely needed. Paleoplacers are known in
682 the Ardennes Upper Famennian (Bocq valley), concentrating Fe-Ti oxides and chromite of mafic
683 magmatism derivation (Goemaere and Hurford (1997). According to Ganssloser (1999), most of the
684 Rhenish metagreywackes of Frasnian to Visean age contain a chromian spinel as a minor component
685 of the heavy mineral spectra, deemed, however, to be sourced in far-sited Alpine-type peridotites.
686 Yet, according to Oncken et al. (1999), this spinel is no longer found to the west of the Rhine graben.
687 Indeed, compared to the east, the western part of the Rhenish massif is characterised by its scarcity
688 in early magmatism, a fact thought by Muchez et al. (2005) to explain the poor endowment in ore
689 deposits of the western Rhenish massif. Although such characteristics would suggest the possibility
690 of some Late Devonian to Carboniferous metasediments containing detrital material that could act
691 as a leachable source of copper (for instance, in Fe-Ti oxides from mafic rocks), it remains that at
692 the erosion level attained in Luxembourg at the onset of Mesozoic sedimentation, all these rocks
693 had already disappeared, thus precluding their potential as source rocks for the copper
694 mineralisation. In the northern Rhenish Massif, low concentrations of stratabound sulphides
695 (interpreted as sedimentary-exhalative) are documented in Lower Carboniferous black shales, and
696 copper, as chalcopyrite, is known at Marsberg and would amount there to about 55 kt Cu, at 1.3 to
697 1.6% Cu (Stribrny et al. 1988). Such a source was eroded at the time of copper deposition and cannot
698 be considered a source for Stolzembourg copper. In the HASB, a small Cu-Mo occurrence is known
699 at Helle, in the Stavelot Massif, as chalcopyrite-molybdenite dissemination and veins within a sill
700 of quartz diorite to tonalite intruded at 381±16 Ma into the Cambrian siliciclastic rocks (Dejonghe
701 2003). In the Lower Ordovician chloritoid-bearing schists, quartz veins with bornite-chalcopyrite-
702 chalcocite mineralisation are known in the Stavelot Massif. They are interpreted as formed at 350°-
703 300°C at the end of the Variscan metamorphism (Hatert 2005). Thus, the Cambro-Ordovician series
704 of the Caledonian basement to the Luxembourg lower Devonian siliciclastics is a possible copper
705 source. This series lies around 1 to 2 km below the copper deposition site, which, given the estimated
706 45°C.km^{-1} gradient, would have reached a temperature close to 230°C necessary to dissolve copper.
707 For the Wenzel deposit in the Black Forest, Staude et al. (2007) also propose the remobilisation of
708 older basement-hosted mineralisations as a source for the Mesozoic ores.
709 On the other hand, the classic view that copper was sourced in the overlying red-beds, as supported
710 in the Black Forest by Staude et al. (2011), is best consistent with the need for oxidising fluid for
711 copper transportation. Yet, to be a valuable source, the red-beds series must include volcano-
712 sedimentary components (bimodal magmatism in rifted areas) or at least a detrital component issued
713 of such series. Yet, LA-ICP-MS analysis of FI in carbonates and fluorite from a deposit (Sailauf,

714 Spessart Crystalline Complex in Germany), where red-bed sourced fluids are documented, failed to
715 find high copper contents in the fluids (Fusswinkel et al. 2014). Such red beds are present in the
716 Vosges and Black Forest districts. Still absent in Luxembourg, the closer area with bimodal
717 components is the Permian Saar-Nahe basin, with its southwestern prolongation beneath the
718 Mesozoic cover, or the Permian Malmédy Graben, in the nearby Stavelot massif (Fig. 1). Presently,
719 the latter is a small structure, 22 km long and 0.5 to 2.5 km wide, with no more than 240 m thick
720 red conglomerates unconformably resting onto the Cambro-Ordovician series of the Stavelot
721 Massif, and fed in detritus by the Devonian of the Eifel massif (Bultynck et al. 2001). These red
722 beds may have reworked some of the potential copper sources in the basement. Finally, although
723 large-scale circulation, possibly through a network of basement faults, is needed, Permian red beds
724 could have constituted the copper source for Stolzembourg.
725
726 ***Age of the Stolzembourg deposit***
727 Stolzembourg is hosted in Lower Pragian rocks, as seen in Fig. 1, at a depth of 2.5 and 1.8 km under
728 the Mesozoic unconformity. Thus, to achieve the 2.8 km depth estimated for the copper deposition
729 at Stolzembourg 300 and 1,000 m of sedimentary cover are required at the time of the mineralisation.
730 This width is roughly consistent with the stratigraphic data. As the final erosion of the cover did not
731 begin before the Miocene, this would imply an earlier date for the mineralising event.
732 Due to the lack of datable material, the age of the Stolzembourg system can be indirectly bracketed
733 because the intense hematisation event must have been related to the deep penetration of surface-
734 derived oxidising water allowing “reddening at great depth along basement fractures”, as described
735 by Cathelineau et al. (2012) on the Poitou High. Deep weathering mantles were frequently
736 developed in Western Europe, starting from the Early Triassic. They show a trend from a
737 kaolinite/ferrallitic style in the Mesozoic to a grussic style in the Tertiary (Migon and Bergström
738 2002). The first event was Permian, in relation to the post-Variscan unconformity. In that
739 Luxembourg area presently corresponding to the Eisleck, where no red-bed deposition of this age
740 seems the rule, such an origin of the wall rock reddening at Stolzembourg may be excluded. A
741 second event, dated from the Early Triassic, is recorded in emerged areas south of Luxembourg, in
742 Swiss (“Vindelician cordillera”: Gisler et al. 2007). Still, at that time, the sedimentary pile was not
743 thick enough to meet the above-discussed requirements. During the Early Cretaceous, in association
744 with major “wavelength deformation” events recorded at the Early Berriasian, and at the end of the
745 Barremian (Guillocheau et al. 2000), a third set of ferricrete was developed. The extensive erosion
746 of the Jurassic limestone platforms on the eastern margin of the Parisian Basin may be attributed to
747 such continent-scale warping and produced kaolinite saprolites and ferricretes, the latter being dated

748 by palaeomagnetism of the Barremian (130±10 Ma, Thiry et al. 2006, Théveniaut et al. 2007). The
749 formation of the calamine zinc deposits from the Ardennes and the northern Rhenish massif can be
750 related to this event. They were formed by oxidation at the expense of former Pb-Zn sulphide veins
751 during the development of an erosion surface with a kaolinite-bearing regolith (Dejonghe and Boni
752 2004), the latter having been dated by Yans (2003) from the Barremian-Aptian (135±15 Ma and
753 126±10 ma, i.e., ca 130 Ma). This event is recorded in the western FMC (Innocent et al. 2019), east
754 of Luxembourg, and Bavaria (c. 125 Ma kaolinite saprolite: Gilg 2000).
755 The wall rock reddening at Solzembourg could thus be related to this third ferricrete event, and early
756 Cretaceous age (Barremian, c 130 Ma) for the Stolzembourg copper mineralisation may, therefore,
757 be proposed with a certain degree of confidence.
758
759 ***Putting the Luxembourg mineralisation in a time and geodynamic context***
760 There is a wealth of absolute chronological data allowing the establishment of a time framework for
761 the fluid circulation events and the related mineralizing episodes, first at the scale of the Upper
762 Rhine graben (taken as a proxy for Luxembourg), then expanded at the western Europe scale: a
763 compilation of available data, in the sedimentary basins and their basement (Appendix A1), and the
764 ore deposits (Appendix A2-3), is summarized in Figure 14.
765 *Evidence for a pulsed activity*
766 Based on illite K/Ar and Ar/Ar dating (Appendix A1) and the evidence for remagnetisation based
767 on palaeomagnetism data (Schott and Peres 1987; Henry et al. 2001; Kechra et al. 2003; Ricordel
768 et al. 2007), it appears that episodic hydrothermal fluid circulation occurred at the same times in the
769 whole of the west European domain, at the boundary between the basement and Permo-Triassic
770 detrital formations (Fig. 14): in the Early and Late Triassic; in the Jurassic during the Lias, then the
771 Malm; in the Cretaceous, during the Neocomian, then the Albo-Aptian, and finally, the Late
772 Cretaceous; at the Cretaceous-Paleogene boundary; and eventually during the Eocene (the latter,
773 only in the Upper Rhine graben). In parallel, the dating of ore deposits, based on various methods
774 and minerals (Appendix A2-3), reveals a pulsed mineralizing activity in broad coincidence with the
775 fluid circulation pattern (Fig. 14).
776 In the best-documented area (the Black Forest, representative of the Upper Rhine graben), after a
777 minor Early Triassic event, three main periods may be distinguished: (i) Jurassic-early Early
778 Cretaceous (Neocomian) for a series of fluorite-barite-quartz-(carbonates) with several substages of
779 Pb-Zn-Ag-Ni-Co-Bi-(Cu) mineralisation, (ii) late Early Cretaceous-Late Cretaceous, for quartz-
780 barite-calcite-(fluorite) with again Pb-Zn-(Cu) and (iii) terminal-Cretaceous-Miocene for barite and
781 Cu-Bi-Pb-Zn mineralisation. These element associations, including Pb-Ag-Bi-Cu, are notably close

782 to that found in the rare luxembourgite ($AgCuPbBi_4Se_8$), described in association with siderite,
783 dolomite and arsenopyrite at Our electric station close to Stolzenbourg (Philippo and Henson, 2007).
784 When other deposits in western Europe are considered, a broadly coincident partition is revealed,
785 with some differences, notably the presence of a limited number of Late Triassic deposits and the
786 minimal occurrences of post-Paleocene deposits (Fig. 14).
787 A very significant fact is the existence of a widespread hydrothermal event in the Late Jurassic (at
788 c 160-145 Ma), with mainly Pb-Zn deposition, which is proved to have coincided with a significant
789 thermal event by fission-track measurements on zircon (Black Forest: Timar-Geng et al. 2004).
790 Everywhere well identified by the radiometric dating, this major event is documented by indirect
791 evidence in areas such as the Ardennes and Rhenish massifs (evidently relevant for comparison with
792 Luxembourg), where the mineralisation is not dated. Thus, the numerous vein-type Pb-Zn deposits
793 and occurrences in the HASB (Fig. 1) are probably related to this Malm event: at least in the Dinant
794 Synclinorium, they pre-date the Cretaceous (Dejonghe 1998; Heijlen et al. 2001). In the northern
795 Rhenish Massif, the Devonian- and Carboniferous-hosted Pb-Zn veins are sealed by "deep phreatic
796 cavities filled with Lower Cretaceous sedimentary rocks" (Drozdzewski et al. 1998, in Götte and
797 Richter 2003). Non-sulphide (calamine) zinc deposits from the Ardennes and the Rhenish massif
798 were formed by oxidation at the expense of former Pb-Zn sulphide veins and related to the
799 development of the Early Cretaceous erosion surface with a kaolinite-bearing regolith (Dejonghe
800 and Boni 2004). It is, therefore, highly probable that the Luxembourg Pb-Zn showings were formed
801 during this Late Jurassic hydrothermal event, as a first barite event as documented at Stolzembourg
802 (cf supra § 5.1).
803 In the Ardennes, paleontologic evidence may be added to the radiometric data. Indeed, the Fleurus
804 barite deposit in the Verviers syncline is dated from the Albian-Aptian by a palynoflora (Demaiffe
805 and Dejonghe 1990, Dejonghe et al. 1987). This is likely to give even more confidence to the
806 attribution of this age to the Stolzembourg copper deposit. A consequence of this attribution is the
807 existence in Luxembourg of the second generation of barite deposition (such as the Biwels system)
808 likely of Cretaceous age as in the Upper Rhine graben. These data equally support the existence of
809 a well-defined Early Cretaceous hydrothermal activity.
810 *Geodynamic constraints on the calendar of hydrothermal activity*
811 As seen in Figure 14, a series of continental-scale tectonic events punctuated the post-Variscan
812 history of Western Europe. They appeared to have coincided broadly with the hydrothermal events
813 they may have monitored. Working at the European plate scale, Burish et al. (2022) concluded that
814 "the formation of Mesozoic vein-hosted and MVT ore deposits is a local expression of geological

processes that happen on a continental scale", and they stressed the importance of rifting to trigger the fluid mixing processes that control ore deposition.

Thus, the Mesozoic events were monitored to a large extent by the rifting and drifting events in both the northern Atlantic and the Tethyan oceanic realms (e.g., Handy et al. 2010, and references therein).

First, the Late Triassic to Liassic events may be correlated with the initiation of the proto-North Atlantic rift system (Sibuet et al. 2012). During the Late Triassic, extensional tectonics were documented in several basins (Dumont 1988), and, at the Trias-Lias boundary, was formed the Central Atlantic Magmatic Province (CAMP), a basaltic LIP developed between 202 and 192 Ma and peaking at c 201 Ma (Marzoli et al. 2018). Indeed, the focus of the responsible mantle plume for the CAMP was located far to the South (between Florida and Senegal). Still, Late Triassic basaltic volcanism is recorded in southern Europe, at the Norian-Rhaetian boundary (c 210 Ma) in the Dauphinois (Dumont 1988) and the Betic belt (Perez-Lopez et al. 2010) and c 200 Ma in Sicily (Cirrincione et al. 2014), meaning that the lithosphere was thermally disturbed much further north than the core zone of the CAMP. The CAMP and related tectonics forecasted the rifting event, active from the Sinemurian to the Early Bajocian (190-170 Ma: Labails et al. 2010).

The major Malm hydrothermal event is related to both the "dramatic change" registered from the Kimmeridgian to the Tithonian in the opening of the Central Atlantic Ocean (Labails et al. 2010) and the coeval North Sea active mantle-driven rifting (Underhill and Partington 1993; Cowie et al. 2005), and the simultaneous opening of the Liguria-Piemont Tethyan oceanic tract starting from the Oxfordian (e.g., Liati et al. 2005; Masini et al. 2013).

The Early Cretaceous hydrothermal events are related to a significant Early Cretaceous extensional event in western Europe (Muchez et al. 2005), which was driven by the westward propagation of oblique hyperextension (up to magma-starved oceanic tracts: Stampfli et al. 2002; Beltrando et al. 2013) along a major transform fault (Handy et al. 2010), from the Valaisan domain to the east (rifting starting at ca 130 Ma: Liati and Froitzheim 2006; Stampfli et al. 2009; Loprieno et al. 2011), to the Pyrenees and the Bay of Biscay to the west (opening beginning as early as 125 Ma, with a peak in the Albian-Cenomanian at 110-95 Ma: Gong et al. 2008; Stampfli et al. 2002; Calvet et al. 2021). Such extensional tectonics could explain the heat input recorded by the FIs in the Stolzembourg deposit, a further argument for the proposed c 130 Ma for the formation of the deposit. The transtensional nature of the Stolzembourg vein system is equally consistent with such an extensional context.

From the very Late Cretaceous onwards, the West European stress state was controlled by the development of the Pyrenees-Alps orogenic wedges. The first Santonian to Maastrichtian

849 ("Laramide") phase of Pyrenean orogenesis (84-68 Ma: Calvet et al. 2021) was apparently of minor
850 importance when hydrothermalism is concerned (Fig. 13). By contrast, the main "Pyreneo-
851 Provençal" phase spanning the Eocene and starting from 55 Ma (Calvet et al. 2021) exerted a
852 considerable influence: compressional stresses exerted on continental Europe by the evolving
853 orogens caused lithospheric buckling and basin inversion up to 1700 km to the north of the Alpine
854 and Pyrenean deformation fronts. This deformation was accompanied by the injection of melilite
855 dykes, reflecting a plume-related increase in the temperature of the asthenosphere beneath the
856 European foreland. Fluid circulation at the continental scale was one of the consequences (Fig. 14).
857 Starting from the Oligocene, the development of the West European rift system was under the
858 control of the ongoing orogenesis in the Alpine domains ("impactogene rifting": Merle and Michon
859 2001). Despite the significant thermal impact revealed by the Tertiary volcanic provinces in the
860 French Massif Central and the Rhenish Massif (Wilson and Downes 2006), the consequences of
861 hydrothermal circulation and mineralizing events were quite limited, being essentially present in the
862 Upper Rhine graben (Fig. 13).
863
864 ***Thermal regimes***
865 An inventory of published data on the Black Forest, Vosges and Ardennes deposits show that during
866 the Mesozoic, recorded fluid temperatures were constantly changing: as shown in Figure 13, fluid
867 mixing occurred at temperatures higher than T_h ranging from 160°C and more, attained for instance
868 at Stolzembourg (this work), Wiesloch (Pfaff et al. 2010), and other Black Forest deposits
869 (Baatartstogt et al. 2007) down to 40°-60°C, recorded for instance by ferroan dolomites occurring
870 in N20°-N30°E extension veins from the Namur Syncline (Muchez et al. 1995), with many
871 carbonates (Nielsen et al. 1998; Walter et al. 2015) and the Pb-Zn in Belgium (Heijlen et al. 2001)
872 being characterised by intermediate temperatures. At a depth of mineralisation of c. 3 km
873 (Stolzembourg: this work, southern Black Forest: Walter et al. 2015) to 1 km (northern Black Forest:
874 Walter et al. 2015), the expected wall rock temperatures would have continuously been lower than
875 100°C owing to the maximal 35°C.km^{-1} geothermal gradients commonly affecting the European
876 crust. The temperatures recorded by the ferroan dolomites from the Namur Syncline (FI T_h between
877 40° and 60°C: Muchez et al. 1995) would be representative of the circulation of fluids thermally
878 equilibrated with their host rocks, as would also be many carbonates from the Black Forest, as well
879 as several barite deposits, and the Pb-Zn showings from Luxembourg at temperatures below 100°C
880 (Fig. 13, lines C and L). Temperatures above 210°C (T_h) recorded in most Pb-Zn, and CaF_2 (and Cu
881 at Stolzembourg) deposits suggest either the transient implementation of abnormal heat flows or the
882 implication of deep fluids, equilibrated under the "normal" thermal gradient but at greater depths,

883 or both. Indeed, combining geochemical thermometry and thermodynamic approaches, it is often
884 proposed that these fluids were initially at temperatures as high as 300°C or more: Deloule (1982)
885 for the Tarn fluorites in French Central Massif, formed at ca 180°-210°C (Munoz et al. 2005), or
886 Pfaff et al. (2010) for the Wiesloch deposit in the Black Forest, formed at $T_h \leq 210$°C. Along the
887 normal gradients, such temperatures would be reached at 9-10 km depth or more. According to
888 Lodemann et al. (1998), the calcic brines found at around 4 km depth in the KTB continental drill
889 hole were transferred into their modern setting from a deeper reservoir at about 9 km depth. There
890 are, however, arguments in favour of transient perturbations of the geothermal gradients.
891 Anisothermal mixing is often observed and records the advection of hot fluids into colder reservoirs,
892 as the model requires. As proposed in Figure 13 (lines S1 and A), this could be a general process,
893 at least for the hotter hydrothermal systems. For instance, in the Wiesloch deposits (late Cretaceous-
894 Paleogene) in the Black Forest, Pfaff et al. (2010) argue for mixing a deep brine equilibrated with
895 the basement at temperatures possibly as high as 300°C but cooled down to ca. 150°C at the
896 deposition site. There, the formation water, initially at no more than 100°C and equilibrated with
897 carbonates, would have been alkaline (pH ca. 8). However, given that the deposit is hosted in the
898 Muschelkalk cover, the temperature of ca 100°C reached by the "low temperature" component
899 requires a high geothermal gradient. In the same way, at Stolzembourg, the colder fluid in the mixing
900 is at c. 140°C, which, if in thermal equilibrium at the estimated c. 3 km depth, would require a
901 48°C.km^{-1} geothermal gradient. It may be observed, by contrast, that the lower T_h recorded by the
902 FI in pre- or post-ore quartz would correspond, under lithostatic conditions, at the same c. 3 km
903 depth, to a temperature of c. 90°C (Fig. 12), yielding, in turn, a less pronounced gradient of 35°C.km^{-1}
904 ^{1}. It, therefore, seems that a transient increase of the regional geothermal gradient characterised the
905 Stolzembourg area at the time of ore formation. Such a conclusion could be extended to the Black
906 Forest deposits and would agree with the extensional context associated with the ore-forming events.
907
908 **Conclusions**
909
910 1. The small Pb-Zn showings in Luxembourg are thought to be equivalent to the Ardennes Pb-Zn
911 deposits. They would consequently have been formed during the Late Jurassic hydrothermal event,
912 associated with the North Atlantic and Ligurian-Piemontese (Thethysian) ocean opening at the
913 Western Europe scale.
914 2. The Stolzembourg copper-only deposit is a likely product of the Mid-Cretaceous thermal event,
915 which affected Western Europe in response to the coeval openings of the Biscaye Bay (to the west)
916 and Valaisan (to the east) oceanic tracts between 130 and 100 Ma. As recorded by fluid inclusions

in syn-chalcopyrite Fe-dolomite, copper ores resulted from the anisothermal mixing from 165°C or more down to 135°C, between two highly saline (ca.27 wt % eq NaCl), brines, one Ca-Na and the other Na-only rich, and low-salinity water. Hydrostatic conditions at an estimated depth of around 3 km are most probable. By contrast, the quartz, which precedes and follows copper deposition, records circulation of lower-temperature brines, interpreted as the result of regional fluid circulation under "normal" geothermal gradients. The copper depositing event thus appears related to a localised transient heat advection produced by the upward migration of brines from a deeper reservoir.

3. Some barite showings in Luxembourg, which post-dated the Stolzembourg ore deposition, must be ascribed to the Late Cretaceous hydrothermal events.

4. Finally, although of little economic importance, the Luxembourg mineral district appears as a missing link between the mineralisation of the Ardennes-Rhenish massifs, on the one hand, and the Upper Rhine graben districts of the Vosges and the Black Forest, on the other.

References

Aldega L, Viola G, Casas-Sainz A, Marcén M, Román-Berdiel T, van der Lelij R (2019) Unraveling Multiple Thermotectonic Events Accommodated by Crustal-Scale Faults in Northern Iberia, Spain: Insights From K-Ar Dating of Clay Gouges. Tectonics 38:3629-3651

Alderton DHM, Selby D, Kucha H, Blundell DJ (2016) A multistage origin for Kupferschiefer mineralization. Ore Geology Reviews 79:535-543

Antun P. 1968. - Die Stölzemburger Kupfererz- gänge: Erwägungen zu ihrer Geologie, Mineralogie und Ausbeutbarkeit. Note interne. Publ. Serv. Géol. de Luxembourg, 28 pp.

Aquilina L, De Dreuzy J-R (2011) Relationships of present saline fluids with paleomigration of basinal brines at the basement/sediment interface (Southeast basin – France). Appl Geochem 26:1933-1945

Baatartsogt B, Schwinn G, Wagner T, Taubald H, Beitter T, Markl G (2007) Contrasting paleofluid systems in the continental basement: a fluid inclusion and stable isotope study of hydrothermal vein mineralization, Schwartzwald district, Germany. Geofluids 7:123-147

Bakker RJ (2003) Package FLUIDS 1. Computer programs for analysis of fluid inclusion data and for modelling bulk properties. Bowers, T.S. and Helgeson, H.C., 1983, Calculation of the thermodynamic and geochemical consequences of nonideal mixing in the system H2O-CO2-

951 NaCl on phase relations in geologic systems. Equation of state for H2O-CO2-NaCl fluids at
952 high pressures and temperatures: Geochim Cosmochimica Acta, v. 47, p. 1247-1275.
953 Brockamp O, Clauer N, Zuther M (2003) Authigenic sericite record of a fossil geothermal system:
954 the Offenburg trough, central Black Forest, Germany. Int J Earth Sci (Geol Rundsch) 92:843-
955 851
956 Brockamp O, Schlegel A, Clauer N (2011) Mesozoic hydrothermal impact on Rotliegende and
957 Bunter immature sandstones of the High Rhine trough and its adjacent eastern area (southern
958 Black Forest, Germany). Sedim Geol 234: 76-88
959 Brockamp O, Schlegel A, Wemmer K (2015) Complex hydrothermal alteration and illite K-Ar ages
960 in Upper Visean molasses sediments and magmatic rocks of the Variscan Badenweiler-
961 Lenzkirch suture zone, Black Forest, Germany. Int J Earth Sci (Geol Rundsch) 104:683-702
962 Bultynck P, Geukens F, Smolderen A (2001) Permian lithostratigraphic units, Malmédy graben
963 (Belgium). Geol Belgica 41:105-106
964 Burisch M, Marks MAW, Nowak M, Markl M (2016) The effect of temperature and cataclastic
965 deformation on the composition of upper crustal fluids - An experimental approach. Chem
966 Geol 433:24-35
967 Burisch M, Markl G, Gutzmer J (2022). Breakup with benefits-hydrothermal mineral systems
968 related to the disintegration of a supercontinent. Earth and Planetary Science Letters, 580,
969 117373
970 Calvet M, Gunnell Y, Laumonier B (2021) Denudation history and palaeogeography of the Pyrenees
971 and their peripheral basins: a 84-million-year geomorphological perspective. Earth Science
972 Reviews 215: 103436
973 Cathelineau M, Fourcade S, Clauer N, Buschaert S, Rousset D, Boiron M-C, Meunier A, Lavastre
974 V, Javoy M (2004) Dating multistage paleofluid percolations: a K-Ar and 18O/16O study of
975 fracture illites from altered Hercynian plutonites at the basement/cover interface (Poitou High,
976 France). Geochim Cosmochim Acta 68:2529-2542
977 Cathelineau M, Boiron M-C, Fourcade S, Ruffet G, Clauer N, Belcourt O, Coulibaly Y, Banks DA,
978 Guillocheau F (2012) A major Late Jurassic fluid event at the basin/basement unconformity
979 in western France: 40Ar/39Ar and K/Ar dating, fluid chemistry, and related geodynamic
980 context. Chem Geol 322-323:99-120
981 Cirrincione R, Fiannacca P, Lustrino M, Romano V, Tranchina A (2014) Late Triassic tholeiitic
982 magmatism in Western Sicily: A possible extension of the Central Atlantic Magmatic
983 Province (CAMP) in the Central Mediterranean area? Lithos 188:60-71

984 Clark ID, Jensen TAM, Kennell L, Mazurek M, Mohapatra R, Raven KG (2013) Paleozoic aged
985 brine and authigenic helium preserved in an Ordovician shale aquiclude. Geology 41:951-954
986 Clauer N, Zwingmann H, Chaudhuri S (1996) Isotopic (K-Ar and oxygen) constraints on the extent
987 and importance of the Liasic hydrothermal activity in Western Europe. Clay Min 31:301-318
988 Clauer N, Weber F, Gauthier-Lafaye F, Toulkeridis T, Sizun J-P (1997) Mineralogical,
989 geochemical(REE) and isotopic (K-Ar, Rb-Sr, □18O) evolution of the clay minerals from
990 faulted, carbonate-rich, passive paleomargin of southeastern Massif Central, France. J Sedim
991 Res 67:923-934
992 Clauer N, Liewig N, Ledesert B, Zwingmann H (2008) Thermal history of Triassic sandstones from
993 the Vosges Mountains-Rhine Graben rifting area, NE France, based on K-Ar illite dating. Clay
994 Min 43: 363-379
995 Cowie P, Underhill J, Behn M, Lin J, Gill C (2005) Spatio-temporal evolution of strain accumulation
996 derived from multi-scale observation of Late Jurassic rifting in the northern North Sea: a
997 critical test of models for lithospheric extension. Earth Planet Sci Lett 234:401-419
998 Debruyne D, Hulsbocsch N, Muchez P (2016) Unravelling rare earth element signatures in
999 hydrothermal minerals using a source-sink system. Ore Geol Rev 72:232-252
1000 Dejonghe L (1998) Zinc-lead deposits of Belgium. Ore Geol Rev 12:329-354
1001 Dejonghe L, Boni M (2004) The “Calamine”-type zinc-lead deposits in Belgium and West
1002 Germany: a product of Mesozoic palaeoweathering processes. Geol Belgica 8:3-14
1003 Dejonghe L, Fairon-Demaret M, Gauthier B, Streel M (1987) Détermination par analyse
1004 palynologique de l’âge crétacé inférieur du gisement de barite de Fleurus (Synclinorium de
1005 Namur, Belgique). C.R. Acad. Sci. Paris 304, II: 227-232
1006 Dejonghe L 2003 The Helle igneous rock and associate porphyry copper mineralization (eastern
1007 Belgium): a summary of the present-day knowledge. Geologica Belgica 6: 43-47
1008 Deloule E (1982) The genesis of fluorspar hydrothermal deposits at Montroc and Le Burc (Tarn)
1009 deduced from the analysis of fluid inclusions. Econ Geol 77:1867-1874
1010 Demaiffe D, Dejonghe L (1990) Géochimie isotopique du strontium des barites, anhydrites, calcites
1011 et fluorites de Belgique. Ann Soc Géol Belgique 113:231-240
1012 Dewaele S, Muchez P, Banks DA (2004) Fluid evolution along multistage composite fault systems
1013 at the southern margin of the Lower Palaeozoic Anglo-Brabant fold belt, Belgium. Geofluids
1014 4:341-356
1015 Dèzes P, Schmid SM, Ziegler PA (2004) Evolution of the European Cenozoic Rift System:
1016 interaction of the Alpine and Pyrenean orogens with their foreland lithosphere.
1017 Tectonophysics 389:1-33

1018 Dill HG, Fricke A, Henning K-H (1995) The origin of Ba- and REE-bearing alumina-phosphate and
1019 sulphate minerals from the Lorheim kaolin clays deposit (Rheiniszche Schiefergebirgen,
1020 Germany). Appl Clay Sci 10:231-245
1021 Dubessy J, Lhomme T, Boiron M-C, Rull F (2002) Determination of chlorinity in aqueous fluids
1022 using Raman spectroscopy of the stretching band of water at room temperature: application to
1023 fluid inclusions. Appl Spectr 56:99-106
1024 Dubois M, Ayt Ougougdal M, Meere P, Royer J-J, Boiron M-C, Cathelineau M (1996) Temperature
1025 of paleo- to modern self-sealing within a continental rift basin; the fluid inclusion data (Soulz-
1026 sous-Forêts, Rhine graben, France). Eur J Miner 8:1065-1080
1027 Dumont T (1988) Late Triassic-Early Jurassic evolution of the western Alps and of their European
1028 foreland; initiation of the Tethyan rifting. Bull Soc Geol France (8) IV: 601-611
1029 Durand M (2014) Le Trias de l'est du Bassin parisien. In: Gély J-P, Hanot F (dir.) and 20 coll., Le
1030 Bassin parisien, un nouveau regard sur la géologie, Bull Inform Géol Bassin Paris, Mém h-
1031 sér 9:50-57
1032 Efimenko N, Schneider J, Spangenberg J, Chiaradia M, Adatte T, Föllmi KB (2014) Formation and
1033 age of sphalerite mineralization in carbonate rocks of Bajocian age in the Swiss Jura
1034 Mountains: evidence of Mesozoic hydrothermal activity. Int J Earth Sci (Geol Rundsch)
1035 103:1059-1082
1036 Fehn U, Snyder GT (2005) Residence times and source ages of deep crustal fluids: interpretation of
1037 129I and 36Cl results from the KTB-VB drill site, Germany. Geofluids 5:45-21
1038 Fielitz W, Mansy J-L (1999) Pre- and syn-orogenic burial metamorphism in the Ardennes and
1039 neighbouring areas (Rhenohercynian zone, central European Variscides). Tectonophysics
1040 309: 227-256
1041 Fluck and Weil 1975
1042 Fusswinkel T, Wagner T, Wälle M, Wenzel T, Heinrich CA, Markl G (2013) Fluid mixing forms
1043 basement-hosted Pb-Zn deposits: insight from metal and halogen geochemistry of individual
1044 fluid inclusions. Geology 41:679-682
1045 Fusswinkel T, Wagner T, Wenzel T, Wälle M, Lorenz J (2014) Red bed and basement sourced fluids
1046 recorded in hydrothermal Mn–Fe–As veins, Sailauf (Germany): A LA-ICPMS fluid inclusion
1047 study. Chemical Geology 363:22-39
1048 Ganssloser M (1999) Detrital chromian spinels in Rhenohercynian greywackes and sandstones
1049 (Givetian-Visean, Variscides, Germany) as indicators of ultramafic source rocks. Geol Mag
1050 136:437-451

1051 Gigoux M, Delpech G, Guerrot C, Pagel M, Augé T, Négrel P, Brigaud B (2015) Evidence for an
1052 Early Cretaceous mineralizing event above the basement/sediment unconformity in the
1053 intracratonic Paris Basin: paragenetic sequence and Sm-Nd data on the world-class Pierre-
1054 Perthuis fluorite deposit. Miner Depos 50:455-463
1055 Gilg HA (2000) D–H evidence for the timing of kaolinization in Northeast Bavaria, Germany. Chem
1056 Geol 170:5-18
1057 Gisler C, Hochuli PA, Ramseyer K, Bläsi H, Schlunegger F (2007) Sedimentological and
1058 palynological constraints on the basal Triassic sequence in Central Switzerland. Swiss J.
1059 Geosc. 100: 263-272
1060 Gleeson SA, Yardley BWD (2002) Extensional veins and Pb-Zn mineralisation in basement rocks:
1061 the role of penetration of formation brines. Water Sci Technol Library Vol 40:189-205
1062 Goemaere E, Hurford AJ (1997) Un paléoplacer dans la Formation d'Evieux (Famennien supérieur)
1063 à Durnal, Vallée du Bocq, Belgique. Ann Soc Géol Belgique 120:133-143
1064 Goh SW, Buckley AN, Lamb RN, Rosenberg RA, Moran D (2006) The oxidation states of copper
1065 and iron in mineral sulfides, and the oxides formed on initial exposure of chalcopyrite and
1066 bornite to air. Geochim Cosmochim Acta 70:2210-2228
1067 Goldstein,R.H., Reynolds,T.J. (1994) Systematics of Fluid Inclusions in Diagenetic Minerals:
1068 SEPM Short Course 31. Society for Sedimentary Geology, 199.
1069 Gong Z, Langereis CG, Mullender TAT (2008) The rotation of Iberia during the Aptian and the
1070 opening of the Bay of Biscay. Earth Planet Sci Lett 273:80-93
1071 Götte T, Richter DK (2003) Late Palaeozoic and Early Mesozoic hydrothermal events in the
1072 northern Rhenish Massif: results from fluid inclusion analyses and cathodoluminescence
1073 investigations. J Geochem Explor 78-79:531-535
1074 Grandia F, Asmerom Y, Getty S, Cardellach E, Canals A (2000) U–Pb dating of MVT ore-stage
1075 calcite: implications for fluid flow in a Mesozoic extensional basin from Iberian Peninsula. J
1076 Geochem Explor 69-70:377-380
1077 Grandjean-Lecuyer P, Feist R, Albarède F (1993) Rare earth elements in old biogenic apatites.
1078 Geochim Cosmochim Acta 57:2507-2514
1079 Guillocheau F, Robin C, Allemand P, Bourquin S, Brault N, Domart G, Friedenv-berg R, Garcia JP,
1080 Gaulier JM, Gaunet F, Grosdoy B, Hanot F, Le Strat P, Nalpas T, Prijac C, Rigollet C, Serrano
1081 O, Grandjean G (2000) Meso-Cenozoic geodynamic evolution of the Paris Basin: 3D
1082 stratigraphic constraints. Geodin Acta 13:189-246

Hagedorn B, Lippolt HJ, Möller P, Lüders V (1993) Isotopic age constraints for epigenetic mineralizations in the Harz Mountains (Germany) from K–Ar, 40Ar/39Ar and Rb–Sr data of authigenic K-feldspars. Monogr Ser Mineral Deposits,

Handy MR, Schmid SM, Bousquet R, Kissling E, Bernouilli D (2010) Reconciling plate-tectonic reconstructions of Alpine Tethys with the geological-geophysical record of spreading and subduction in the Alps. Earth-Sci Rev 102:121-158

Hatert F (2005) Transformation sequences of copper sulphides at Vielsam, Stavelot Massif, Belgium. Can Miner 43:623-635

Hautmann S, Lippolt HJ (2000) 40Ar/39Ar dating of central European K-Mn oxides – a ch/sediment unconformity in the Paris Basin: paragenetic sequence and Sm-Nd data on the world-class Pierre-Perthuis stratabound fluorite deposit chronological framework of supergene alteration processes during the Neogene. Chem Geol 170:37-80

Hecht L, Freiberger R, Gilg HA, Grundmann G, Kostitsyn Y (1999) Rare earth elements and isotope (C, O, Sr) characteristics of hydrothermal carbonates: genetic implications for dolomite-hosted talc mineralization at Göpfersgrün (Fichtelgebirge, Germany). Chem Geol 155:115-130

Heijlen W, Muchez P, Banks D, Nielsen P (2000) Origin and geochemical evolution of synsedimentary, syn- and post-tectonic high-salinity fluids at the Variscan thrust front in Belgium. J Geochem Explor 69-70:149-152

Heijlen W, Muchez P, Banks DA (2001) Origin and evolution of high-salinity, Zn-Pb mineralising fluids in the Variscides of Belgium. Miner Depos 36:165-176

Heijlen W, Muchez P, Banks DA, Schneider J, Kucha H, Keppens E (2003) Carbonate-hosted Zn-Pb deposits in Upper Silesia, Poland: origin and evolution of mineralizing fluids and constraints on genetic models. Econ Geol 98:911-932

Henry B, Rouvier H, Le Goff M, Leach D, Macquar J-C, Thibieroz J, Lewchuk MT (2001) Palaeomagnetic dating of widespread remagnetization on the southeastern border of the French Massif Central and implications for fluid flow and Mississippi Valley-type mineralization. Geoph J Internat 145:368-380

Ingebritsen SE, Manning CE (2010) Permeability of the continental crust: dynamic variations inferred from seismicity and metamorphism. Geofluids 10:193-205

Innocent C, Girard J-P, Wyns (2019) A likely lower cretaceous age for the palaeo- lateritic formations of the Saint-Maixent-l'Ecole graben (Poitou saddle) as indicated by a Rb-Sr, delta O-18-delta D and U-Th isotopic study of ferrugineous pisoids. Bull Soc Géol Fr 190, 10.1051/bsgf/2018018

1117 Izart A, Barbarand J, Michels R, Privalov VA (2016) Modelling of the thermal history of the
1118 Carboniferous Lorraine coal basin: consequences for coal bed methane. Int J Coal Geol
1119 168:253-274
1120 Jochum J (2000) Variscan and post-Variscan lead-zinc mineralization, Rhenish Massif, Germany:
1121 evidence for sulfide precipitation via thermochemical sulfate reduction. Miner Depos 35:451-
1122 464
1123 Johannesson KH, Lyons WB, Yelken MA, Gaudette HE, Stetzenbach KJ (1996) Geochemistry of
1124 the rare-earth elements in hypersaline and dilute acidic natural terrestrial waters: complexation
1125 behaviour and middle rare-earth elements enrichments. Chem Geol 133:125-144
1126 Jowet, E.C., Pearce, G.W., Rydzewski, A. (1987) A Mid-Triassic Paleomagnetic age of the
1127 Kupferschiefer Mineralizatio in Poland, Based on a Revised Apparent Polar Wander Path for
1128 Europe and Russia. Journal of Geophysical Research 92, B1 : 581-598
1129 Karg H, Carter A, Brix MR, Littke R (2005) Late- and post-Variscan cooling and exhumation
1130 history of the northern Rhenish massif and the southern Ruhr Basin: new constraints from
1131 fission-track analysis. Int J Earth Sci (Geol Rundsch) 94:180-192
1132 Kechra F, Vandamme D, Rochette P (2003)Tertiary remagnetization of normal polarity in Mesozoic
1133 marly limestones from SE France. Tectonophysics 362:219-238
1134 Kirnbauer T, Wagner T, Taubald H, Bode M (2012) Post-Variscan hydrothermal vein
1135 mineralization, Taunus, Rhenish Massif (Germany): constraints from stable and radiogenic
1136 isotope data. Ore Geol Rev 48:239-257
1137 Köhler SJ, Harouiya N, Chairat C, Oelkers EH (2005) Experimental studies of REE fractionation
1138 during water-mineral interactions: REE release rates during apatite dissolution from pH 2.8 to
1139 9.2. Chem Geol 222:168-182
1140 Konrad HJ, Wachsmut W (1973) Zur Lithologie und Tektonik des Unterdevons im südlichen
1141 Oesling Luxemburgs. Publ. Serv. Géol. Luxembourg, Bull. N°5. 20 Pp.
1142 Labails C, Olivet J-L, Aslanian D, Roest WR (2010) An alternative early opening scenario for the
1143 Central Atlantic Ocean. Earth Planet Sci Lett 297:355-368
1144 Lev SM, McLennan SM, Meyers WJ, Hanson GN (1998) A petrographic approach for evaluating
1145 trace-element mobility in a black shale. J Sedim Res 68:970-980
1146 Liati A, Froitzheim N (2006) Assessing the Valais ocean, Western Alps: U-Pb SHRIMP zircon
1147 geochronology of eclogite in the Balma unit, on top of the Monte Rosa nappe. Eur J Miner
1148 18:299-308

Liati A, Froitzheim N, Fanning CM (2005) Jurassic ophiolites within the Valais domain of the Western and Central Alps: geochronological evidence for re-rifting of oceanic crust. Cont Miner Petr 149:446-461

Lodemann M, Fritz P, Wolf M, Ivanovich M, Hansen BT, Nolte E (1999) On the origin of saline fluids in the KTB (Continental Deep Drilling Project of Germany). Appl Geochem 13:656-671

Longerich, H.P., Jackson, S.E., Günther, D., 1996. Laser ablation inductively coupled plasma mass spectrometric transient signal data acquisition and analyte concentration calculation. JAAS 11, 899-904.

Loprieno A, Bousquet R, Bucher S, Ceriani S, Dalla Torre FH, Fügenschuh B, Schmid SM (2011) The Valais units in Savoy (France): a key area for understanding the palaeogeography and the tectonic evolution of the Western Alps. Intern J Earth Sc 100: 963-992

Louvat D, Michelo J-L, Aranyossy J-F (1999) Origin and residence time of salinity in the Aspö groundwater system. Appl Geochem 14:917-925

Markl G, Keim MF, Bayer R, (2019) Unusual mineral diversity in a hydrothermal vein-type deposit: the Clara mine, SW Germany, as a type example. Canad Mineral 57:427-456

Marzoli A, Callegaro S, Dal Corso J, Davies J.H.F.L., Chiaradia M, Youbi N, Bertrand H, Reisberg L, Merle R, Jourdan F (2018) Chapter 4: The Central Atlantic Magmatic Province (CAMP): A Review. In: Tanner L.H. (ed.), The Late Triassic World, Topics in Geobiology 46, Springer International Publishing AG 2018:92-1

Masini E, Manatschal M, Mohn G (2013) The Alpine Tethys rifted margins: reconciling old and new ideas to understand the stratigraphic architecture of magma-poor rifted margins. Sedimentology 60:174-196

Mei Y, Sherma, DM, Liu W, Brugger J (2013) Ab initio molecular dynamics simulation and free energy exploration of copper (I) complexation by chloride and bisulfide in hydrothermal fluids. Geochi Cosmochim Acta 102:45-64

Merle O, Michon L (2001) The formation of the West European Rift; a new model as exemplified by the Massif Central area. Bulletin de la Société Géologique de France 172: 213-221

Mertz DF, Karpenko MI, Ivanenko VV, Lippolt NJ (1991) Evidence for Jurassic tectonism in the Schartzwald basement (SW Germany) by laser probe 40Ar/39Ar dating of authigenic feldspar. Naturwissenschaften 78:411-413

Meyer M, Brockamp O, Clauer N, Renk A, Zuther M (2000) Further evidence for a Jurassic mineralizing event in central Europe: K-Ar dating of hydrothermal alteration and fluid

1182 inclusion systematics in wall rocks of the Käfersteige fluorite vein deposit in the northern
1183 Black Forest, Germany. Miner Depos 35:754-761
1184 Migon P, Bergström KL (2002) Deep weathering through time in central and northwestern Europe:
1185 problems of dating and interpretation of geological record. Catena 49: 25-40
1186 Möller P, Lüders V, Schröder J, Luck J (1991) Element partitioning in calcite as a function of
1187 solution flow rate: a study on vein calcites from the Harz Mountains. Miner Depos 26:175-
1188 179
1189 Möller P, Woith H, Dulski P, Lüders V, Erzinger J, Kämpf H, Pekdeger A, Hansen B, Lodemann
1190 M, Banks D (2005) Main and trace elements in KTB-VB fluid: composition and hints to its
1191 origin. Geofluids 5:28-34
1192 Mosar J. 1992. - Structures et dynamique dans l'Ardenne luxembourgeoise vues dans le cadre d'une
1193 tectonique chevauchante. Structural Geology, Eislek, Luxembourg. Projet de Recherche
1194 R&D/BFR/89012-A1. Rapport Final 126 pp.
1195 Muchez P, Slobodnik M, Viaene WA, Keppens E (1995) Geochemical constraints on the origin and
1196 migration of palaeofluids at the northern margin of the Variscan foreland, southern Belgium.
1197 Sediment Geol 96:191-200
1198 Muchez P, Heijlen W, Banks D, Blundell D, Boni M, Grandia F (2005) Extensional tectonics and
1199 the timing and formation of basin-hosted deposits in Europe. Ore Geol Rev 27:241-267
1200 Muchez P, Hulsbosch N, Heijlen W (2022) Age dating of sediment-hosted ore deposits: new insights
1201 from U-Pb age dating of carbonates from the Polish MVT deposits. In: Proceedings of the
1202 16th SGA Meeting: 267-271
1203 Munoz M, Wayne RP, Courjault-Radé P (2005) Sm-Nd dating of fluorite from the world-class
1204 Montroc fluorite deposit, southern Massif Central, France. Miner Depos 39:970-975
1205 Navarro-Ciurana D, Domènech M, Cardellach E, Corbella M (2018) A Cretaceous-Tertiary
1206 Hydrothermal Event in the Atlantic-Tethys margin? Evidences from MVT Ores and
1207 Paleomagnetism. Macla (Revista Soc Esp Miner) 23
1208 Négrel P, Casanova J, Brulhet J (2006) REE and Nd isotope stratigraphy of a late Jurassic carbonate
1209 platform, eastern Paris Basin, France. J Sedim Res 76:605-617
1210 Nielsen P, Swennen R, Muchez P, Keppens E (1998) Origin of Dinantian zebra dolomites south of
1211 the Brabant-Wales Massif, Belgium. Sedimentology 45:727-743
1212 Nierhoff R, Clauer N, Spaeth G (2011) New findings on the tectono-metamorphic history of the
1213 western Rhenish Massif (Germany) by K-Ar dating of metasedimentary illite. J Geodyn
1214 52:129-142

1215 Ohr M, Halliday AN, Peacor DR (1994) Mobility and fractionation of rare earth elements in
1216 argillaceous sediments: implications for dating diagenesis and low-grade metamorphism.
1217 Geochim Cosmochim Acta 58:289-312
1218 Oncken O, von Winterfeld C, Dittmar U (1999) Accretion of a rifted passive margin: the Late
1219 Paleozoic Rhenohercynian fold-and-thrust belt (Middle European Variscides). Tectonics
1220 18:75-91
1221 Pearce, N.J.G., Perkins, W.T., Westgate, J.A., Gorton, M.P., Jackson, S.E., Neal, C.R., Chenery,
1222 S.P., 1997. A Compilation of New and Published Major and Trace Element Data for NIST
1223 SRM 610 and NIST SRM 612 Glass Reference Materials. Geostandards and Geoanalytical
1224 Research 21, 115-144.
1225 Peng J, Hu R, Burnard PG (2003) Samarium-neodymium isotope systematics of hydrothermal
1226 calcites from the Xikuangshan antimony deposit (Hunan, China): the potential of calcite as a
1227 geochronometer. Chem Geol 200:129-136
1228 Pérez-López A, Pérez-Valera F, Götz AE (2012) Record of epicontinental platform evolution and
1229 volcanic activity during a major rifting phase: The Late Triassic Zamoranos Formation (Betic
1230 Cordillera, S Spain). Sedimentary Geology 247-248:39-57
1231 Pfaff K, Romer RL, Markl G (2009) U-Pb ages of ferberite, chalcedony, agate, “U-mica” and
1232 pitchblende: constraints on the mineralization history of the Schartzwald ore district. Eur J
1233 Miner 21:817-836
1234 Pfaff K, Hildebrandt LH, Leach DL, Jacob DE, Markl G (2010) Formation of the Wiesloch
1235 Mississippi Valley-type Zn-Pb-Ag deposits in the extensional setting of the Upper
1236 Rhinegraben, SW Germany. Miner Depos 45:647-666
1237 Philippo S, Hanson A (2007) La minéralisation en antimoine de Goesdorf. Ferrantia 49:111-146
1238 Philippo, S, Hatert F. (2018) La minéralisation en antimoine de Goesdorf (2). Ferrantia , 77, 7-66
1239 Philippo S, Hoffmann I, Faber A, Heinen G, Schoellen J, Schroeder N, Luc B, Bornain S (2007) La
1240 mineralisation en cuivre de Stolzembourg. Ferrantia 49:7-99
1241 Philippo S, Kronz G (2007) Une seconde occurrence mondiale de gravegliaite et une première
1242 occurrence nationale d’or, Schimpach, Grand-Duché de Luxembourg. Ferrantia 49:101-110
1243 Piqué A, Canals A, Grandia F, Banks DA (2008) Mesozoic fluorite veins in NE Spain record
1244 regional base metal-rich brine circulation through basin and basement during extensional
1245 events. Chem Geol 257:139-152
1246 Pryvalov, V., Pironon, J., Izart, A., Michels, R., Panova, O. (2015) A new tectonic model for the
1247 Late Paleozoic evolution of the Lorraine-Saar coal-bearing basin (France/Germany).
1248 Тектоніка і стратиграфія 2015, вип. 42: 40-50

Richard et al., 2003

Richard A, Pettke T,l Cathelineau M, Boiron M-C, Mercadier J, Cuney M, Derome D (2010) Brine–rock interaction in the Athabasca basement (McArthur River U deposit, Canada): consequences for fluid chemistry and uranium uptake. Terra Nova 22: 303-308

Ricordel C, Parcerisa D, Thiry M, Moreau MG, Gómez-Gras D (2007) Triassic magnetic overprints related to albitization in granites from the Morvan massif (France). Palaeogeogr Palaeoclimatol Palaeoecol 251: 268–282

Rongemaille E, Bayon G, Pierre C, Bollinger C, Chu N-C, Fouquet Y, Riboulot V, Voisset M (2011) Rare earth elements in cold seep carbonates from the Niger delta. Chem Geol 286:196-206

Roth S (2003) Geochemical signature of rocks and weathering products in Luxembourg. PhD Bonn University, 108 pp

Schaltegger U, Corfu F (1995) Late Variscan "Basin and Range" magmatism and tectonics in the Central Alps: evidence from U-Pb geochronology. Geodinamica Acta, 8:82-98

Schärer U, de Parseval P, Polvé M, de Saint Blanquat M (1999) Formation of the Trimouns talc-chlorite deposit (Pyrenees) from persistent hydrothermal activity between 112 and 97 Ma. Terra Nova 11: 30-37

Schlegel A, Brockamp O, Clauer N (2007) Response of clastic sediments to episodic hydrothermal fluids in intramontane trough: a case study from Black Forest, Germany. Eur J Miner 19:833-848

Schleicher AM, Warr LN, Kober B, Laverret E, Clauer N (2006) Episodic mineralization of hydrothermal illite in the Soultz-sous-Forêts granite (Upper Rhine Graben, France). Cont Miner Petr 152:349-364

Schneider J, Haack U, Stedingk K (1999) Direct Rb-Sr dating of sansdstone-hosted sphalerites from stratabound Pb-Zn deposits in the northern Eifel, NW Rhenish Massif, Germany. In: Stanley CJ et al. (eds), Mineral deposits: Processes to processing, Proceedings Vth SGA Meeting, London, Balkema, Rotterdam: 1287-1290

Schneider J, Haack U, Stedingk K (2003) Rb-Sr dating of epithermal vein mineralization stages in the eastern Harz Mountains (Germany) by paleomixing lines. Geochim Cosmochim Acta 67:1803-1819

Schott JJ, Peres A (1987a) Paleomagnetism of the Lower Cretaceous redbeds from northern Spain: evidence for a multistage acquisition of magnetization. Tectonophysics 139:239-253

1281 Schott JJ, Peres A (1987b) Paleomagnetism of Permo-Triassic Redbeds from the Asturias and
1282 Cantabric Chain (northern Spain): evidence for strong lower Tertiary remagnetizations.
1283 Tectonophysics 140:179-191
1284 Schwinn G, Markl G (2005) REE systematics in hydrothermal fluorite. Chem Geol 216:225-248
1285 Schwinn G, Wagner T, Baatartsogt B, Markl G (2006) Quantification of mixing processes in ore-
1286 forming hydrothermal systems by combination of stable isotope and fluid inclusion analyses.
1287 Geochim Cosmochim Acta 70:965-982
1288 Sibuet J-C, Rouzoc S, Srivastava S (2012) Plate tectonic reconstructions and paleogeographic maps
1289 of the Central and North Atlantic oceans. Revue Canadienne des Sciences de la Terre 49
1290 :1395-1415
1291 Sintubin et al.2008
1292 Su W, Hu R., Xia B, Xia Y, Liu Y (2009) Calcite Sm-Nd isochron age of the Shuiyindong Carlin-
1293 type gold deposit, Guizhou, China. Chem Geol 258:269-274
1294 Stampfli GM, Borel GD, Marchant R, Mosar J (2002) Western Alps geological constraints on
1295 western Tethyan reconstructions. In: Rosenbaum G, Lister GS (eds), reconstruction of the
1296 evolution of the Alpine-Himalayan Orogen. J Virtual Explorer 7:75-104
1297 Stampfli GM, Hochard C (2009) Plate tectonics of the Alpine realm. In: Murphy JB, Keppie JD,
1298 Hynes AJ (eds) Ancient orogens and modern analogues, Geol Soc London Spec Publ 327:89-
1299 111
1300 Staude S, Bons P, Markl G (2009) Hydrothermal vein formation by extension-driven dewatering of
1301 the middle crust: an example from SW Germany. Earth Planet Sci Lett 286:387-395
1302 Staude S, Wagner T, Markl G (2007) Mineralogy, mineral compositions and fluid evolution at the
1303 Wenzel hydrothermal deposit, southern Germany: implications for the formation of
1304 Kongsberg-type silver deposits. Can Miner 45:1147-1176
1305 Staude S, Göb S, Pfaff K, Ströbels F, Premo WR, Markl G (2011) Deciphering fluid sources of
1306 hydrothermal systems: a combined Sr- and S-isotope study on barite (Schwartzwald, SW
1307 Germany). Chem Geol 286:1-20
1308 Staude S, Mordhost T, Nau S, Pfaff K, Brügmann G, Jacob DE (2012 a) Hydrothermal carbonates
1309 of the Schwarzwald ore district, southwestern Germany: carbon source and conditions of
1310 formation using □18O, □13C, 87Sr/86Sr, and fluid inclusions. Canad Miner 50:1401-1434
1311 Staude S, Werner W, Mordhorst T, Wemmer K, Markl G (2012 b) The complex multi-stage
1312 Wittichen Co-Ag-Bi-U and Cu-Bi hydrothermal veins, Schwartzwald, SW Germany: tectonic
1313 control and quantitative conditions of mineralization. Miner Depos 47:251-276

1314 Staudt E. 1977. - La distribution des indices de cuivre dans les Ardennes belges et luxembour-
1315 geoises. Travail de fin d'étude pour l'obtention du grade d'ingénieur civil géologue,
1316 Université de Liège, 138 p.
1317 Steele-MacInnis M, Bodnar RJ, Naden J (2011) Numerical model to determine the composition of
1318 H2O-NaCl-CaCl2 fluid inclusions based on microthermometric and microanalytical data.
1319 Geochim Cosmochim Acta 75:21-40
1320 Stollhofen H, Bachmann GH, Barnasch J, Bayer U, Beutler G, Franz M, Kästner M, Legler B,
1321 Mutterlose J, Radies D (2008) Upper Rotliegend to Early Cretaceous basin development. In:
1322 Littke R, Bayer U, Gajewski D, Nelskamp S (eds), Dynamics of complex intracontinental
1323 basins: the Central European Basin system, Springer, Ch 4.3:181-209
1324 Stribrny B, Urban H, Weber H (1988) The Lower Carboniferous black shale formation, a possible
1325 source for noble and base metal deposits in the NE Rhenish Massif, Federal Republic of
1326 Germany. Miner Petr 39:129-143
1327 Ströbele F, Staude S, Pfaff K, Premo WR, Hildebrandt LH, Baumann A, Pernicka E, Markl G (2012)
1328 Pb isotope constraints on fluid flow and mineralization processes in SW Germany. N Jb Miner
1329 Abh 189:287-309
1330 Symons DTA, Lewchuk MT, Kawasaki K, Velasco F, Leach DL (2009) The Reocín zinc–lead
1331 deposit, Spain: paleomagnetic dating of a late Tertiary ore body. Miner Deposita 44:867-880
1332 Symons DTA, Kawasaki K, Walther S, Borg G (2011) Paleomagnetism of the Cu–Zn–Pb-bearing
1333 Kupferschiefer black shale (Upper Permian) at Sangerhausen, Germany. Miner Deposita
1334 46:137-152
1335 Théveniaut H, Quesnel F, Wyns R, Hugues G (2007) Palaeomagnetic dating of the "Borne de Fer"
1336 ferricrete (NE France): Lower Cretaceous continental weathering. Palaeogeography,
1337 Palaeoclimatology, Palaeoecology 253: 271–279
1338 Thierry J, Dugué O, Hanzo M (2014) Le Bassin parisien au Jurassique. In: Gély J-P, Hanot F (dir.)
1339 and 20 coll., Le Bassin parisien, un nouveau regard sur la géologie, Bull Inform Géol Bassin
1340 Paris, Mém h-sér 9:58-74
1341 Thiry M, Quesnel F, Yans J, Wyns R, Simon-Coinçon R (2006) Continental France and Belgium
1342 during the early Cretaceous: paleoweatherings and paleolandforms. Bull Soc Géol France
1343 177:155-175
1344 Thornton MM, Wilson AM (2007) Topography-driven flow versus buoyancy-driven flow in the
1345 U.S. midcontinent: implications for the residence time of brines. Geofluids 7:69-78

Timar-Geng Z, Fügenschuh B, Schalteger U, Wetzel A (2004) The impact of the Jurassic hydrothermal activity on zircon fission tracks data from the southern Upper Rhine Graben area. Schweiz Miner Petr Mitteil 84:257-269

Tissot CL (1967) Influence de la température et de la pression sur la formation des hydrocarbures dans les argiles à kérosène. 7th World Petroleum Congress, Mexico City, Mexico, p 14

Tricca A, Stille P, Steinmann M, Kiefel B, Samuel J, Eikenberg J (1999) Rare earth elements and Sr and Nd isotopic compositions of dissolved and suspended loads from small river systems in the Vosges mountains (France), the river Rhine and groundwater. Chem Geol 160:139-158

Truche L, Bazarkina EF, Barré G, Thomassot E, Berger G, Dubessy J, Robert P (2014) The role of S3- ion in thermochemical sulphate reduction: geological and geochemical implications. Earth Planet Sci Lett 396:190-200

Ulrich MR, Bodnar RJ (1988) Systematics of stretching fluid inclusions. II. Barite at one atmosphere confining pressure. Econ Geol 83:1037-1046

Underhill JR, Partington MA (1993) Jurassic thermal doming and deflation in the North Sea: implications of the sequence stratigraphic evidence. Geol Soc, London, Petrol Geol Conf Ser 4:337-345

Wagner T, Cook NJ (2000a) Late-Variscan antimony mineralisation in the Rheinisches Schiefergebirge, NW Germany: evidence for stibnite precipitation by drastic cooling of high-temperature fluid systems. Miner Depos 35:206-222

Wagner T, Schneider J (2002) Lead isotope systematics of vein-type antimony mineralization, Rheinisches Schiefergebirge, Germany: a case history of complex reaction and remobilization processes. Miner Depos 37:185-197

Walter BF, Burisch M, Markl G (2016) Long-term chemical evolution and modification of continental basement brines – a field study from the Schwarzwald, SW Germany. Geofluids 16:604-623

Walter BF, Immenhauser A, Geske A, Markl G (2015) Exploration of hydrothermal carbonate magnesium isotope signatures as tracers for continental fluid aquifers, Schwarzwald mining district, SW Germany. Chem Geol 400:87-105

Walter BF, Burisch M, Marks MAW, Markl G (2017) Major element compositions of fluid inclusions from hydrothermal vein-type deposits record eroded sedimentary units in the Schwarzwald district, SW Germany. Miner Deposita 52:1191-1204

Walter BF, Burisch M, Fusswinkel T, Marks MAW (2018a) Multi-reservoir fluid mixing processes in rift-related hydrothermal veins, Schwarzwald, SW-Germany. J Geochem Explor 186:158-186

Walter BF, Gerdes A, Kleinhanns IC, Dunkl I, von Eynatten H, Kreissl S, Gregor Markl G (2018b) The connection between hydrothermal fluids, mineralization, tectonics and magmatism in a continental rift setting: Fluorite Sm-Nd and hematite and carbonates U-Pb geochronology from the Rhinegraben in SW Germany. Geochim Cosmochim Acta 240: 11-42

Walter BF, Jensen JL, Coutinho P, Laurent O, Markl G, Steele-MacInnis M (2020) Formation of hydrothermal fluorite-hematite veins by mixing of continental basement brine and redbed-derived fluid: Schwarzwald mining district, SW- Germany. J Geochem Expl 212:106512

Wernicke RS, Lippolt HJ (1997) Evidence of Mesozoic multiple hydrothermal activity in the basement at Nonnenmattwheiler (southern Schwarzwald), Germany. Miner Depos 32:197-200

Wilson M, Downes H (2006) Tertiary-Quaternary intra-plate magmatism in Europe and its relationship to mantle dynamics. In: Gee DG, Stephenson R (eds.) European lithosphere dynamics. Geol Soc London Mem 32: 147-166

Xiao Z., Gammons CH, William-Jones AE (1998) Experimental study of copper (I) chloride complexing in hydrothermal solutions at 40 to 300°C and saturated water vapour pressure. Geochim Cosmochim Acta 62:2949-2964

Yans J (2003) An overview of the saprolites of Belgium and their potential kaolinic supplies to Mesozoic and Cainozoic sediments. Géol France 1:33-37

Ziegler PA, Dèzes P (2007) Cenozoic uplift of Variscan Massifs in the Alpine foreland: timing and controlling mechanisms. Global Planet Change 58:237-269

Zwing A, Clauer N, Liewig N, Brachtadse V (2009) Identification of remagnetization processes in Paleozoic sedimentary rocks of the northeast Rhenish Massif in Germany by K-Ar dating and REE tracing of authigenic illite and Fe oxides. J Geophys Res 114, B6, doi:10.1029/2008JB006137

Figure captions

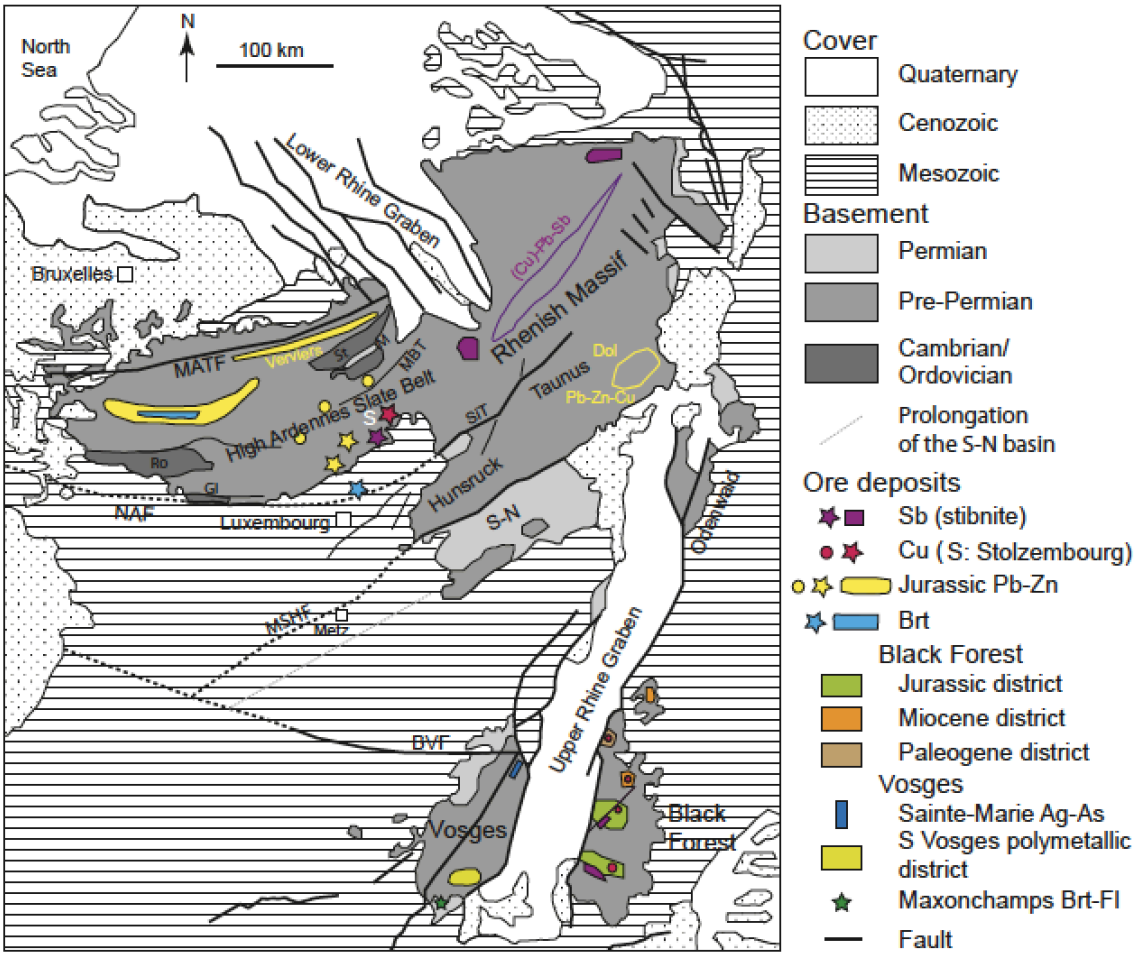

Figure 1. Luxembourg ore deposits and occurrences in their regional context. Geology adapted from France 1/1 000 000 geological map (BRGM), Timar-Geng et al. (2006), Sintubin et al. (2008) and Pryvalov et al. (2015). The Sb deposits are taken from Baatartsogt et al. (2007) (Black Forest) and Wagner and Cook (2000) (Hunsrück). Pb-Zn-(Cu) deposits from the Hunsrück are taken from Kirnbauer et al. (2012), while Pb-Zn-Ba deposits from the Ardennes (Verviers syncline, etc.) are taken from Dejonghe (1998). The Black Forest Pb-Zn-F-Ba and polymetallic districts are taken from Baatartsogt et al. (2007), Staude et al. (2009) and Ströbele et al. (2012). Vosges deposits are from Fluck and Weil (1975). Pre-Devonian inliers in the Ardennes belt: Gi Givonne, Ro Rocroi, St Stavelot. Permian basins: M Malmedy, S-N Saar-Nahe. Faults: BVF Bray-Vittel fault, MBT Malsbenden back thrust, MFAT Midi Fault-Aachen thrust, MSHF Metz-South Hunsrück fault, NAF North Artois fault, SiT Siegen thrust.

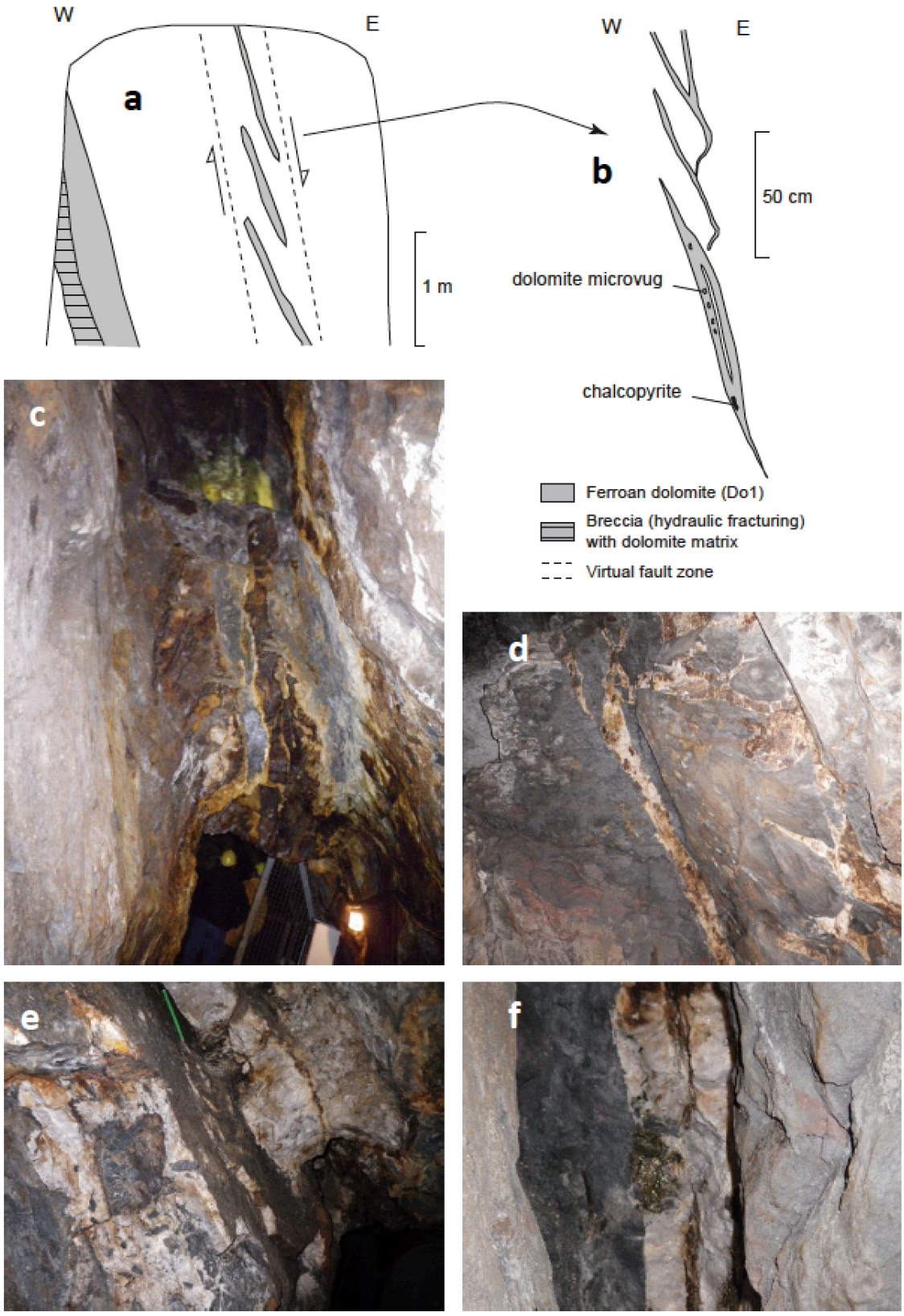

Figure 2. a, b: Carbonate veins structure at Stolzembourg, drawing from the level 1 gallery. c, d: photographs of the level 1 addit; e,f details of the vein infilling: e: breccia cemented by dolomite, f: chalcopyrite in a subvertical dolomite infilling.

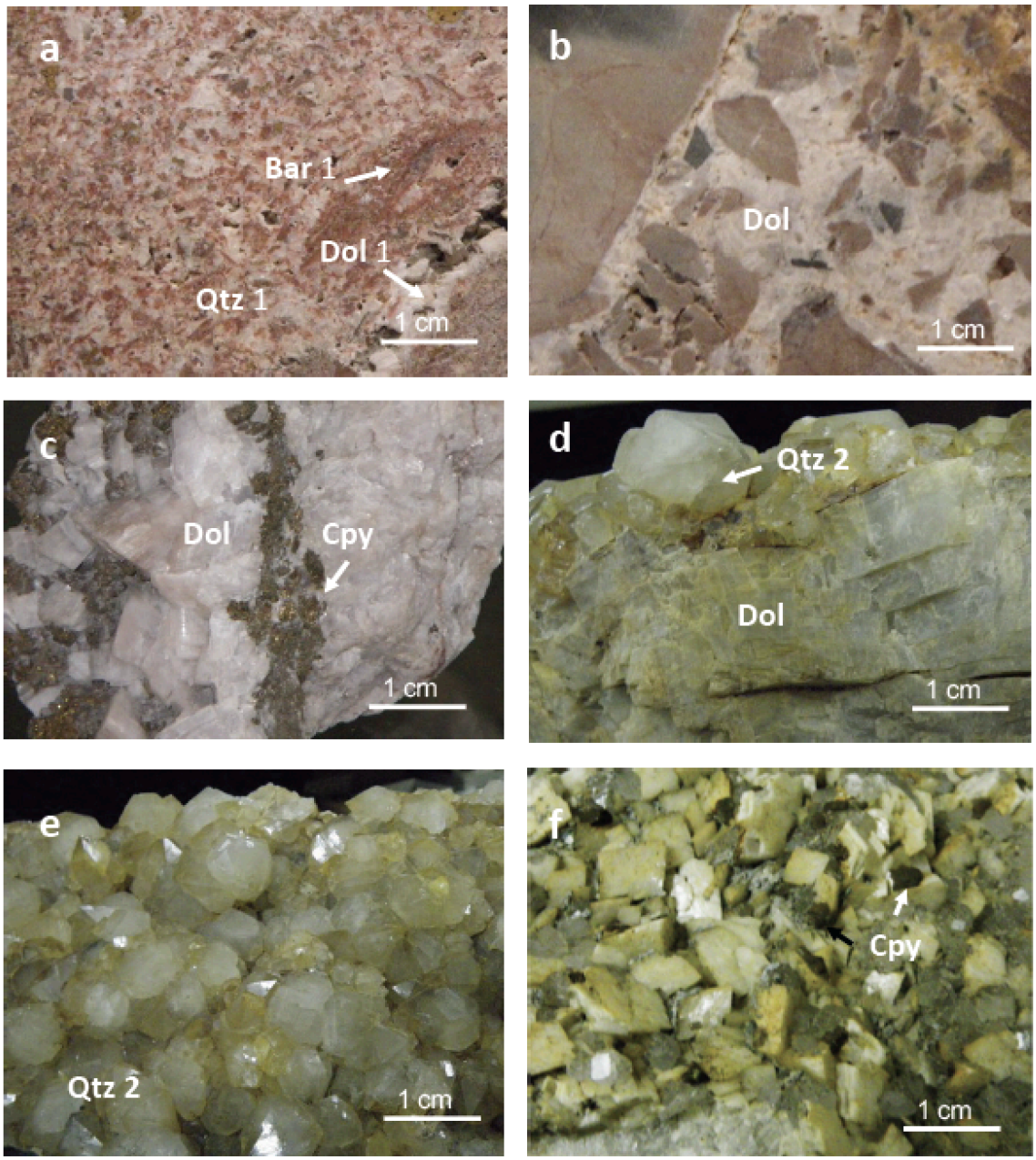

Figure 3: Macrophotographs of ore samples. a: red ore with quartz (Qtz1), dolomite (Dol 1) and barite (Bar1); b: breccia cemented by dolomite; c: large dolomite crystals and chalcopyrite; d: Dolomite covered by euhedral bi-terminated euhedral quartz crystals (Qtz2), e: late infilling of euhedral quartz (Qtz2), f: euhedral dolomite crystals covered by chalcopyrite nodules.

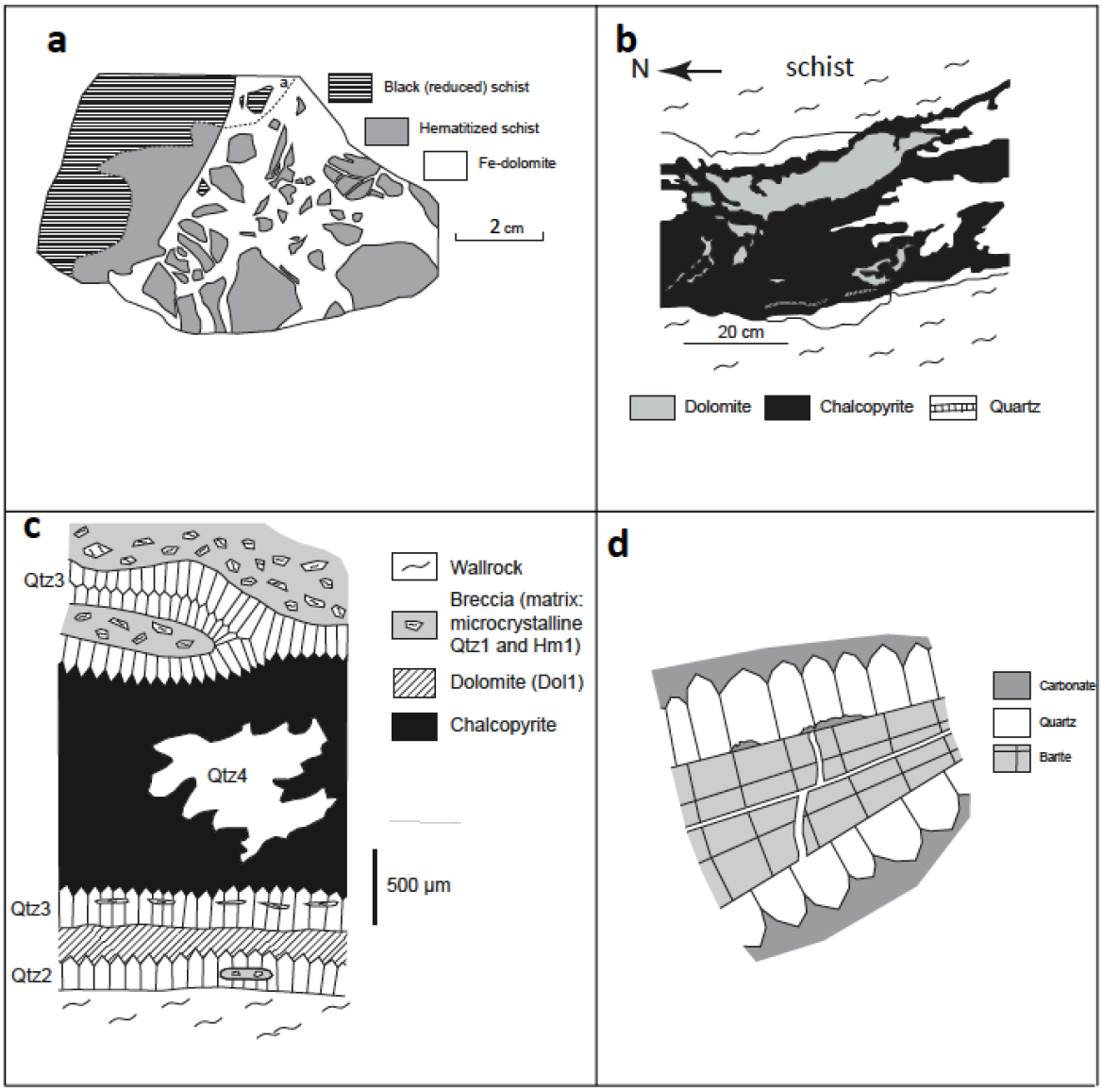

Figure 4. a) Drawing of a Stolzembourg mine sample from the MnhnL collection (ZA109), illustrating the early reddening of the country-rock schists before hydraulic fracturing and the formation of the dolomite-cemented breccia. The dotted line "a" marks the boundary between reduced and oxidised schists as established before the inception of hydraulic fracturing. b) Ore texture at the vein scale in the Stolzembourg mine, at level 1 (redrawn from Philippo et al. 2007). c) Sketch drawing of a mineralized vein from the Riedgerbësch exploration drive at Stolzembourg. d) Drawing of a thin section in a barite sample (ZA094) from the Stolzembourg mine.

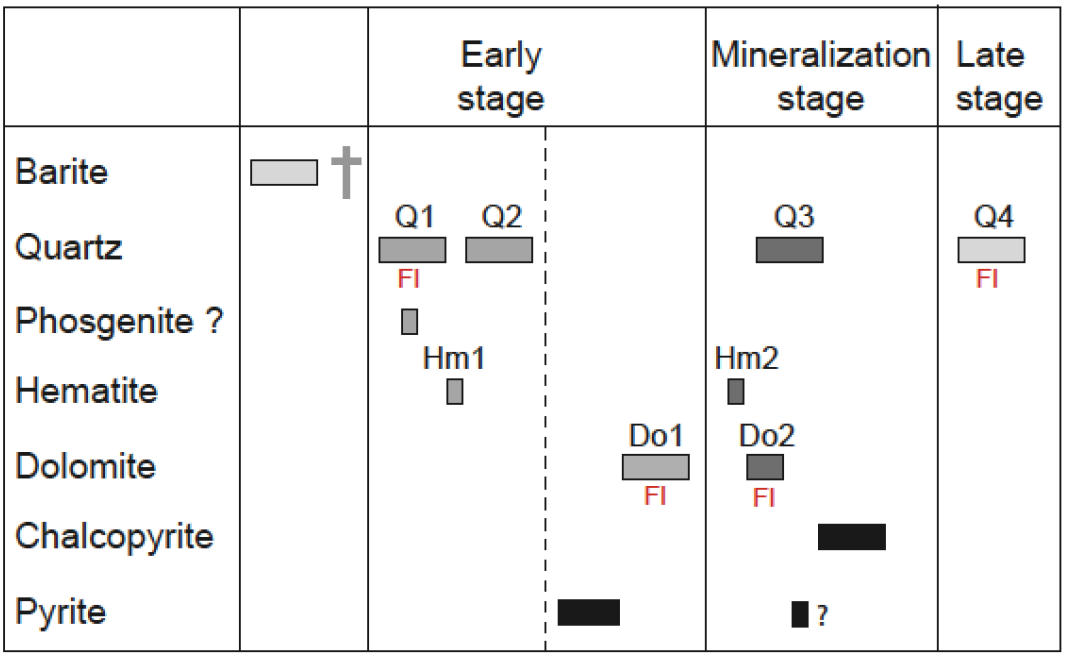

1439

1440 Figure 5 Paragenetic succession at the copper mine of Stolzembourg.

1441

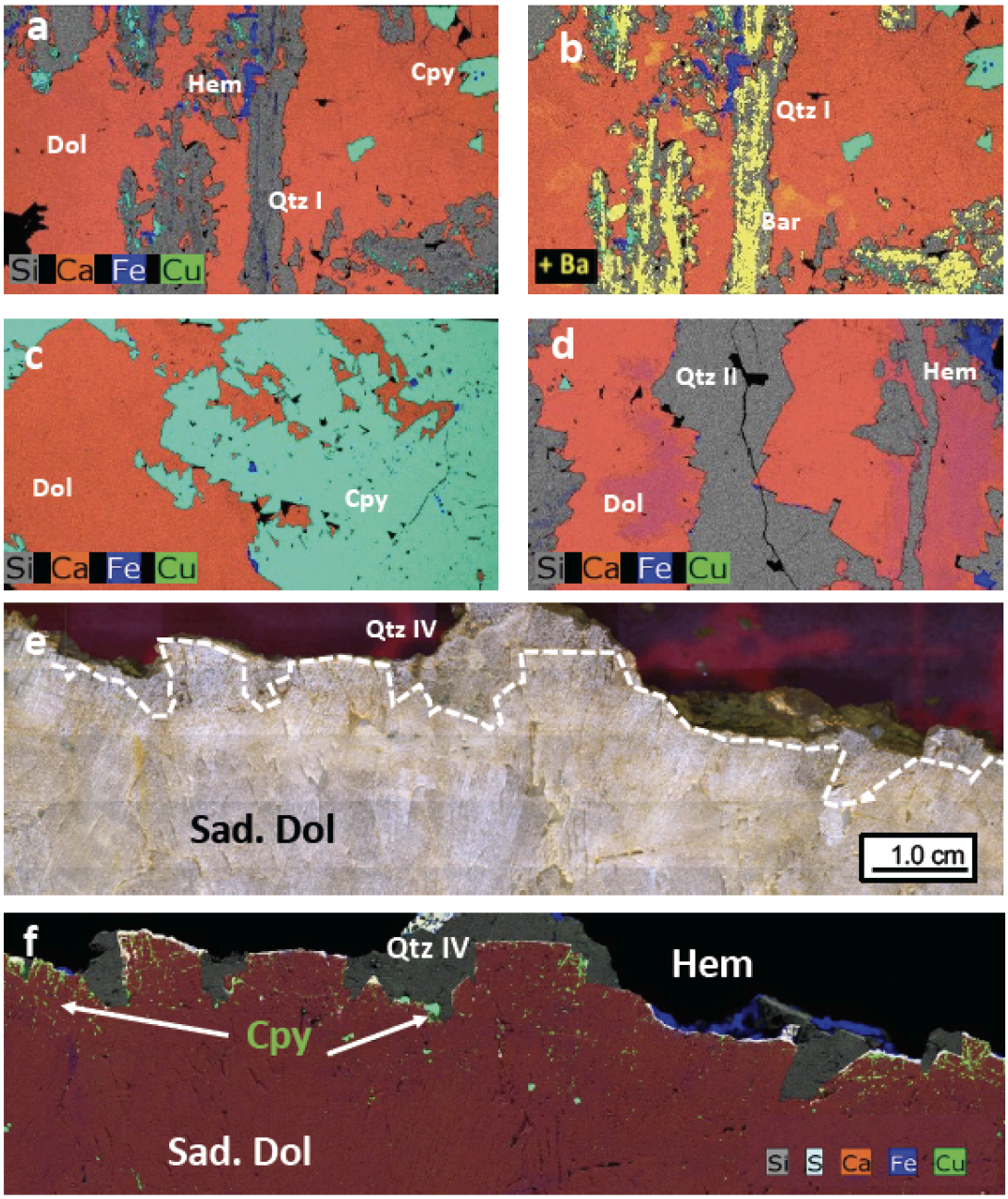

Figure 6: MicroXRF maps of element distribution. a) red ore: association quartz (Qtz 1), dolomite (Dol 1), chalcopyrite, hematite; b) barite partly replaced by quartz, included in dolomite; c) relationships between dolomite and chalcopyrite, d: dolomite with microdomains enriched in iron (same sample as c); d) euhedral dolomite and quartz (Qtz3) infillings; e: macrophotograph of saddle dolomite covered by euhedral quartz Qtz 4; f: microXRF image of the same sample showing chalcopyrite grains in the late growth band and below Qtz4.

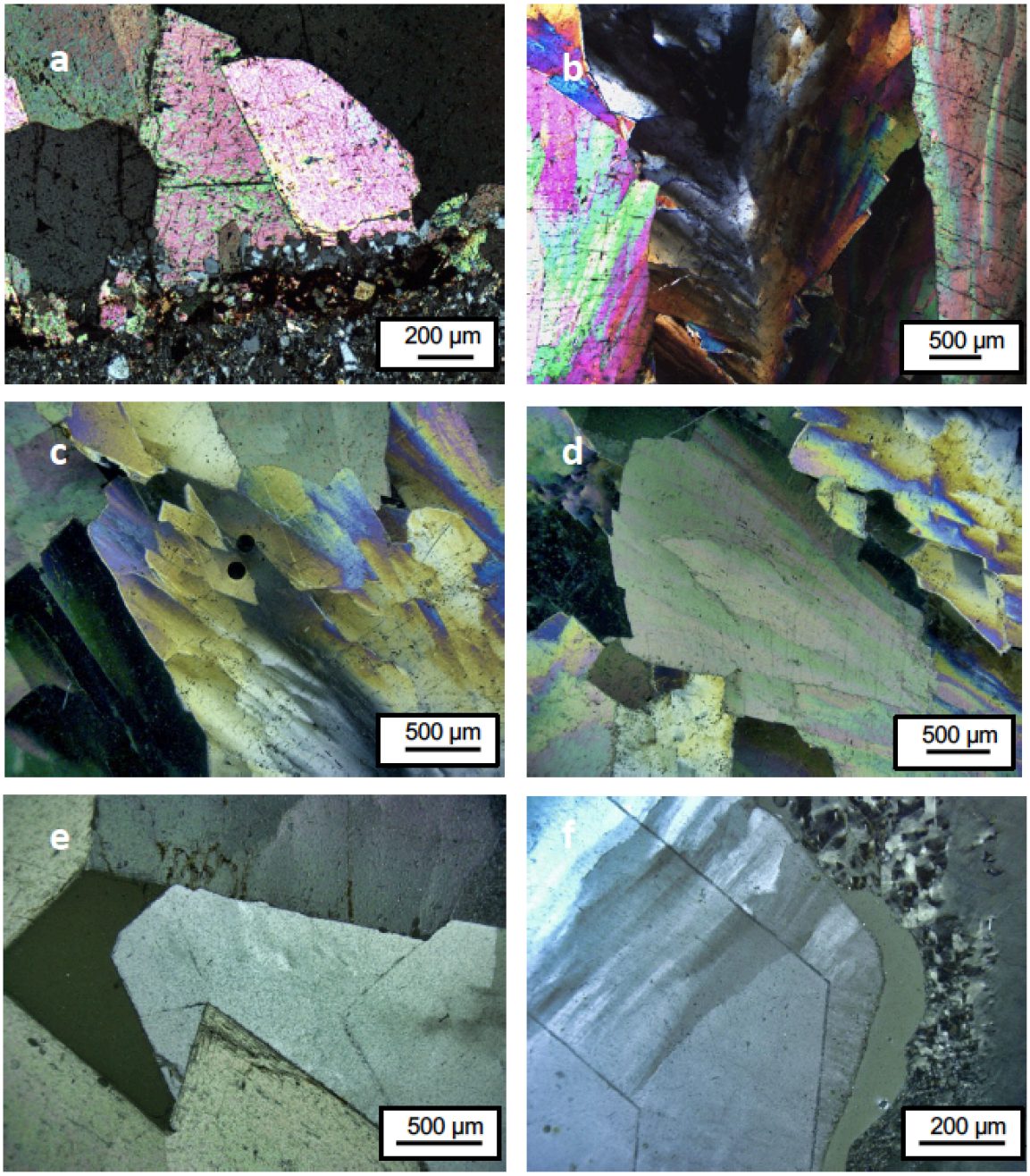

Figure 7. Microphotographs of quartz-dolomite assemblage. a: quartz (Qtz 2) preceding dolomite (Dol 1), b: plumose dolomite crystals, saddle dolomite 2, c: saddle dolomite 2 with craters of LA-ICP-MS analyses (black dots), d: saddle dolomite crystals, e: euhedral quartz Qtz 4 over saddle dolomite 2, f: quartz growth bands of Qtz 4.

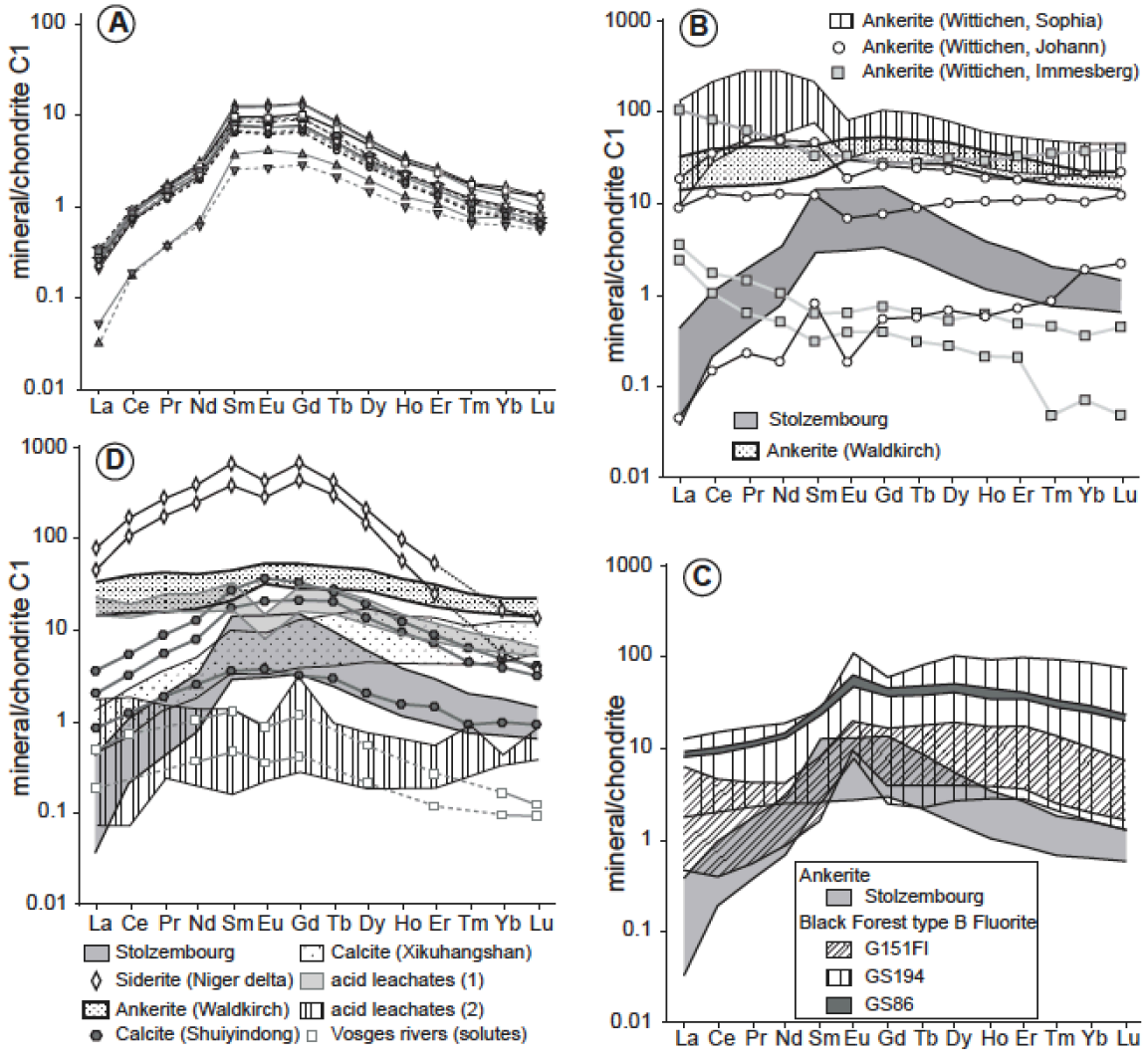

Figure 8. REE data for the Stolzembourg dolomite and comparison with a selection of similar data. A: REE spidergrams of the Stolzembourg dolomites. B: comparison of the Stolzembourg REE patterns with a selection of Black Forest ankerites (data from Staude et al. .2012 a). C: comparison of the Stolzembourg REE pattern with a selection of Black Forest fluorites (data from Schwinn and Markl 2005). D: Comparison of the Stolzembourg REE patterns with a selection of carbonates from other deposits worldwide (data from Peng et al. 2003; Shu et al. 2009; Rongemaille et al. 2011) and with the results of experimental (Ohr et al. 1994) and natural (Tricca et al. 1999) leaching. The dolomite REE contents are normalized to the C1 chondrite (Anders and Grevesse 1989).

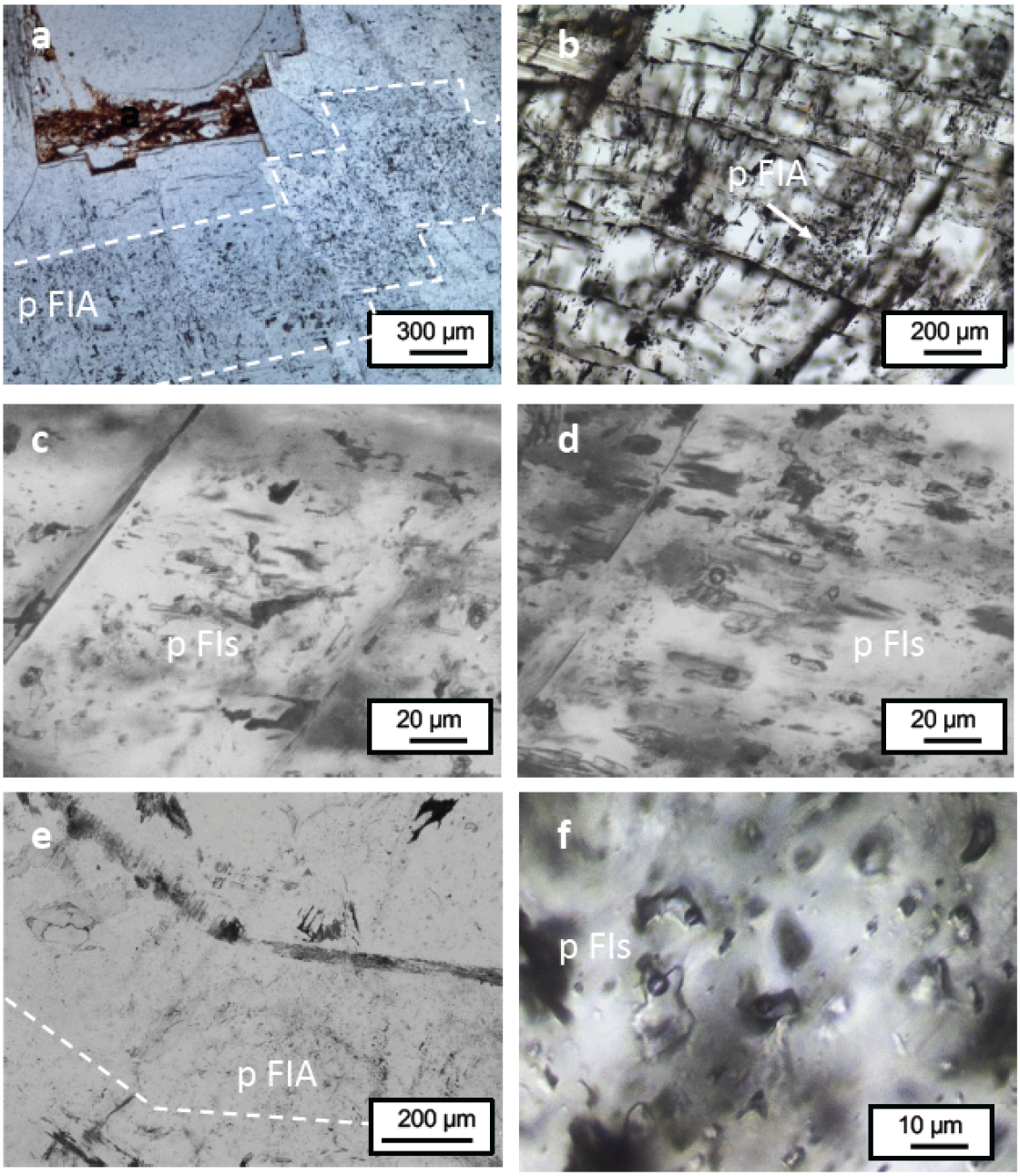

Figure 9: Fluid inclusions assemblages in quartz and dolomite from the main Stolzembourg vein. a: distribution of primary FIA (p FIA) in growth bands of saddle dolomite; b: location of p FIA in dolomite growth bands; c: two-phase FIA, Lw in dolomite; d: two-phase FIA, Lw in dolomite showing elongated shapes with edges subparallel to the main crystallographic orientation; e: growth band in quartz Q2 with primary FIs cluster (p FIA); f: primary two-phase FIs in quartz Q4.

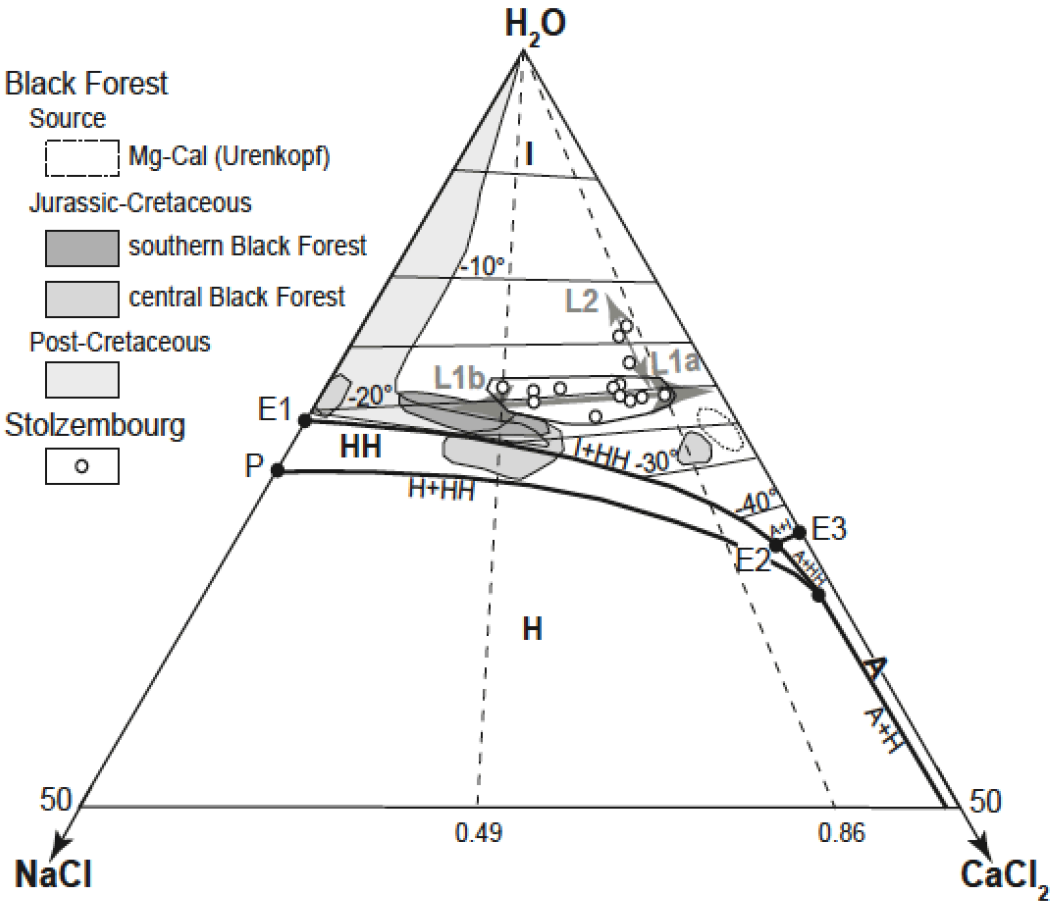

Figure 10: Estimated compositions of the Stolzembourg brines from dolomite and quartz, in the H_2O-NaCl-$CaCl_2$ system (phase diagram adapted from Bodnar 2003). Phase fields and cotectic labelling: A antarcticite, H halite, HH hydrohalite, I ice; eutectic points: E1 H_2O-NaCl-$CaCl_2$, E2 H_2O-NaCl, E3 H_2O-$CaCl_2$; P: H_2O-NaCl peritectic point. Most hydrohalite melting temperatures ($T_{m\,hh}$) were obtained for high salinity FI (with similar low $T_{m\,ice}$ around -20°C), displaying evidence (very variable Na to Ca ratios) for a mixing trend between two fluid poles (L1a and L1b). The few $T_{m\,hh}$ measured in lower salinity FI suggest the existence of a trend toward the H_2O pole, possible evidence for a mixing trend between the L1 brines and a low-salinity L2 fluid.

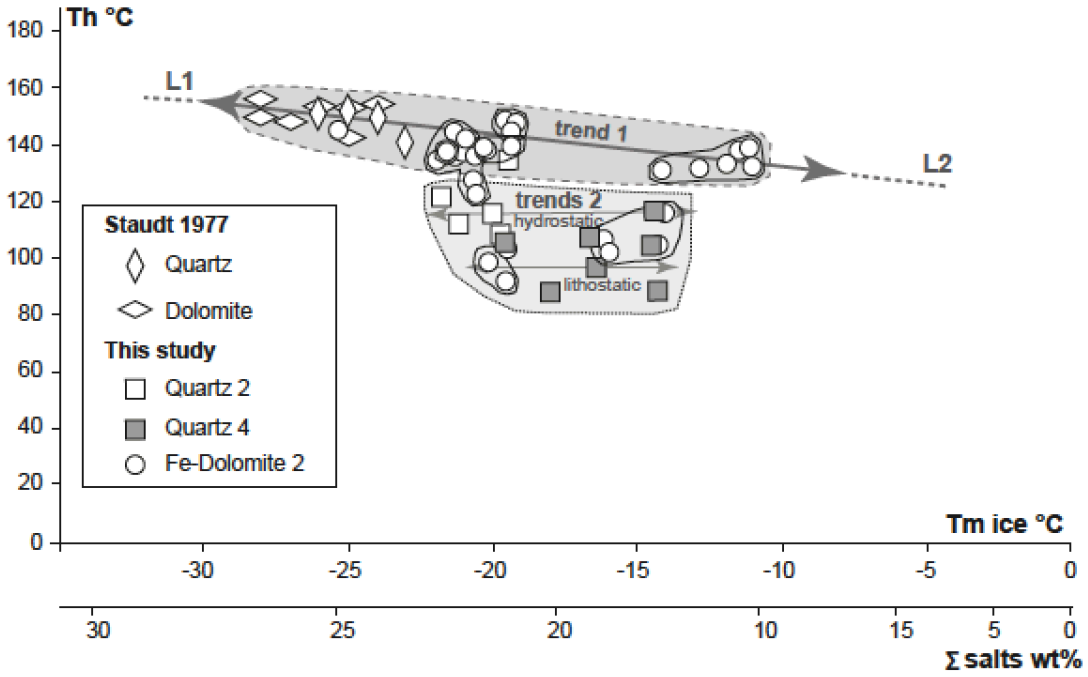

Figure 11. T_h-$T_{m\ ice}$ (bulk salinity) diagram for the Stolzembourg fluid inclusions in Stolzembourg quartz and dolomite. Individual FIs are plotted. Two trends may be defined based on the main host for the FI, either the Fe-dolomites (trend 1) or the quartz (trend 2). These trends may be interpreted as mixing trends. See the text for an explanation.

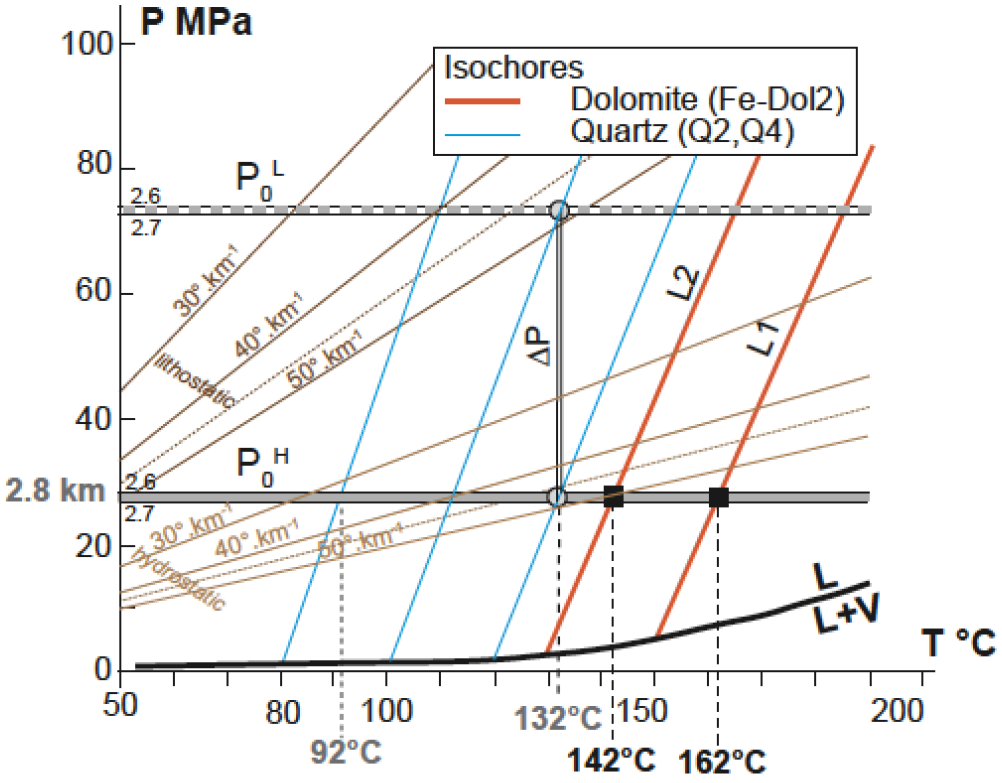

Figure 12. Isochores of the Stolzembourg fluid inclusions and estimation of the P-T trapping conditions. P_0^H: estimated hydrostatic pressure during copper ore formation; P_0^L: corresponding lithostatic pressure. See the text for an explanation.

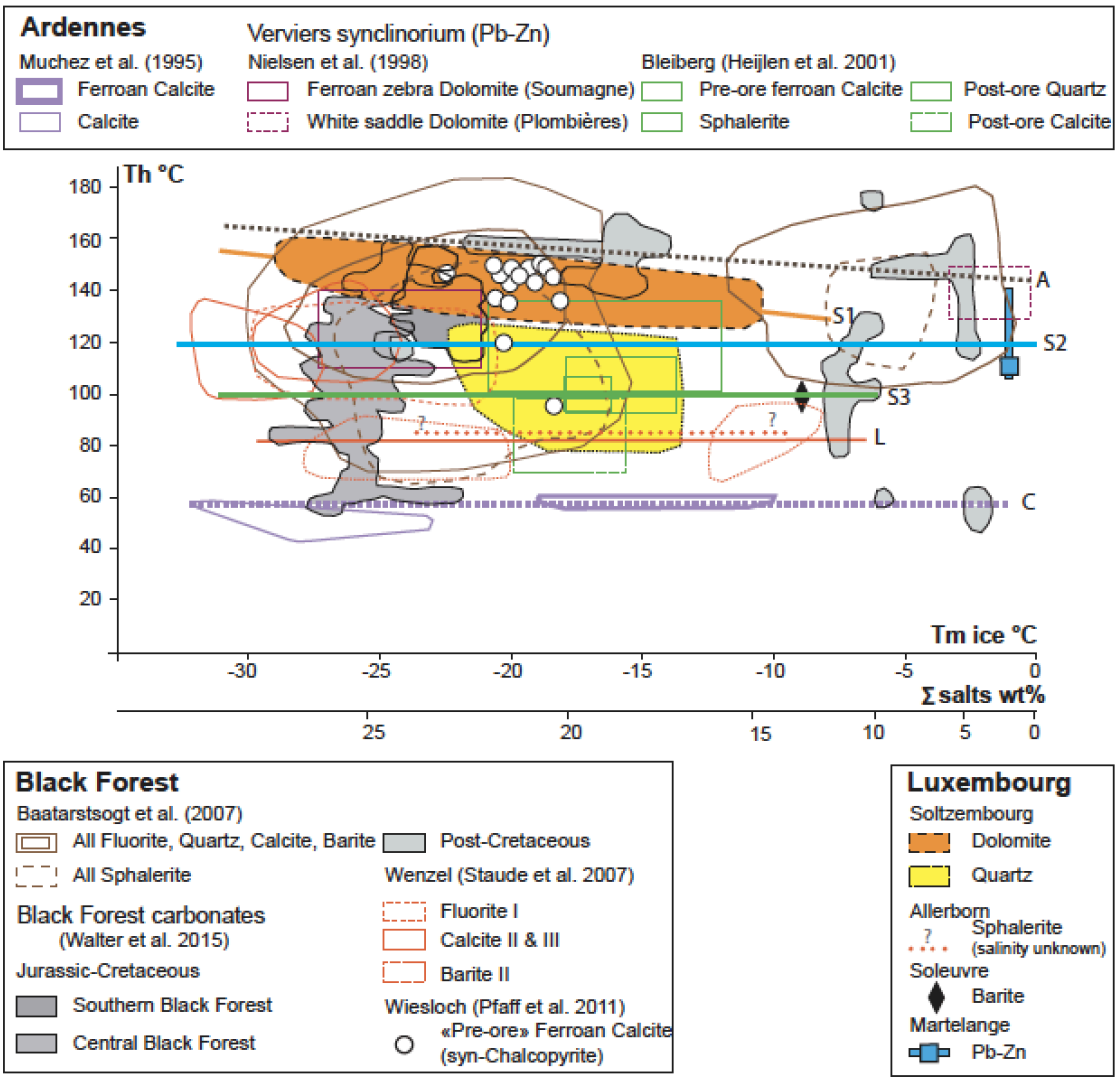

Figure 13. Comparison of Luxembourg fluids with mineralizing fluids from various districts in the Ardennes and the Black Forest in a T_h-$T_{m\ ice}$ (or bulk salinity) diagram. When necessary, bulk salinity in published diagrams was converted into Tm ice. All these fluids are Ca-rich, but as the Ca/Na ratio usually remains unknown (due to a lack of pertinent microthermometric data), the bulk salinity-Tm ice bijection was calculated from Steele-MacInnis et al. (2011) for an arbitrary 0.5 value of the $XCaCl_2$ parameter. The mixing trends observed at Stolzembourg lines S1 to S3 in the figure are seen to be representative (i) of some other Luxembourg deposits and (ii) of many deposits from both the Ardennes and the Black Forest; in particular, the Wesloch deposit data appear to fit the S1 trend associated with Cu deposition. A line A drawn parallel to S1 seems to be able to explain the highest T_h measured in several deposits. The line L, drawn close to the measured temperature at Allerborn, is also possibly representative of a

series of Black Forest data. Finally, a low-temperature mixing trend (line B) is present in the Ardennes and the Black Forest.

1510

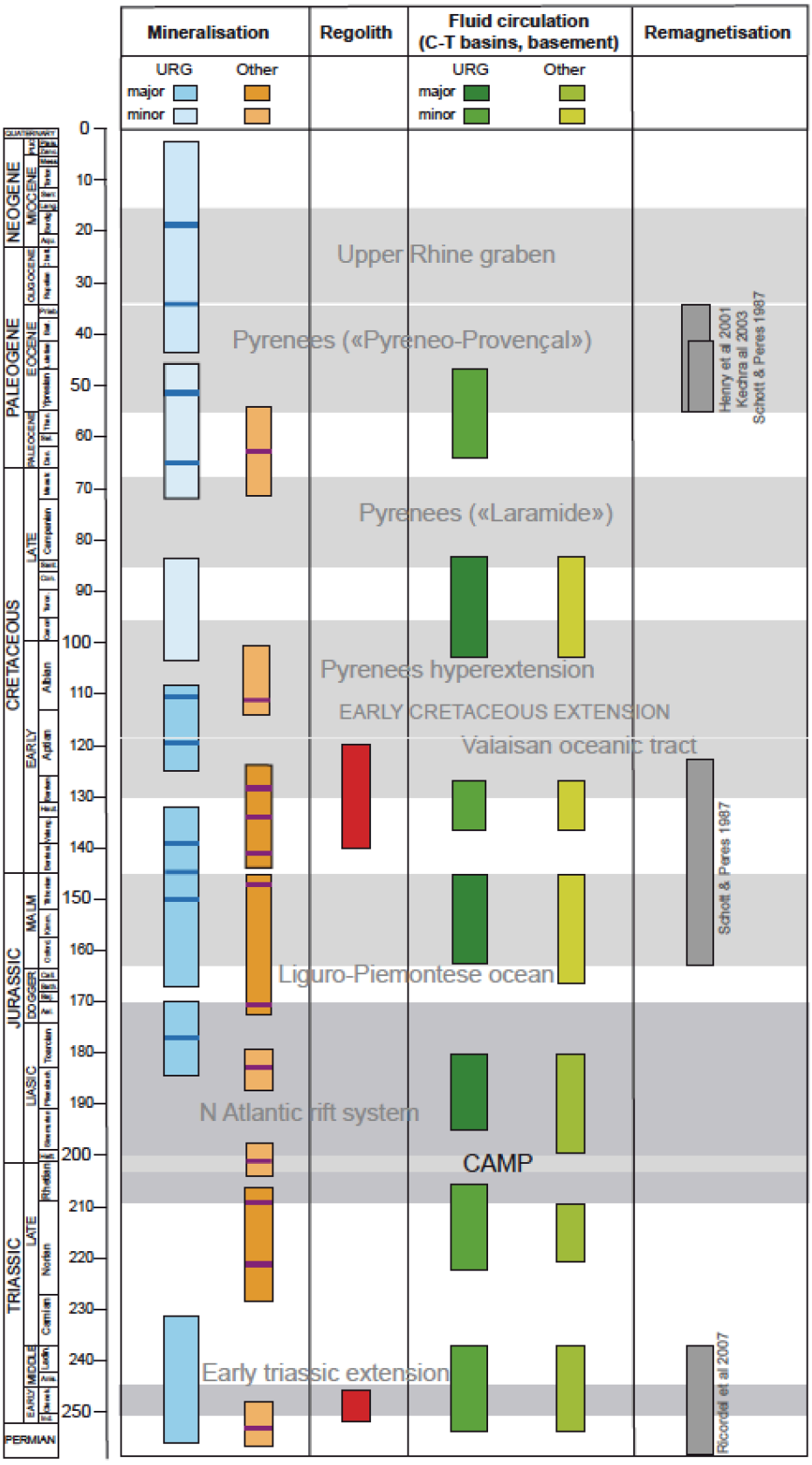
Mineralisation
Regolith
Fluid circulation (C-T basins, basement)
Remagnetisation
URG
Other
major
minor
URG
Other
major
minor
Upper Rhine graben
Pyrenees («Pyreneo-Provençal»)
Pyrenees («Laramide»)
Pyrenees hyperextension
EARLY CRETACEOUS EXTENSION
Valaisan oceanic tract
Liguro-Piemontese ocean
N Atlantic rift system
CAMP
Early triassic extension
Henry et al 2001
Kechra al 2003
Schott & Peres 1987
Schott & Peres 1987
Ricordel et al 2007
NEOGENE
PALEOGENE
CRETACEOUS
JURASSIC
TRIASSIC
PERMIAN
0
10
20
30
40
50
60
70
80
90
100
110
120
130
140
150
160
170
180
190
200
210
220
230
240
250

1511

Figure 14. A synthetic time framework for the fluid circulations in sedimentary basins and their basements and the associated mineralizing episodes at the Upper Rhine graben (URG) and western Europe scales. Explanations in the text; see Appendix A2-3 for more details. Data are from: Aldega et al. (2016); Alderton et al. (2016); Brockamp et al. (2003, 2011, 2015); Cathelineau et al. (2004, 2012); Clauer et al. (1996, 2008); Efimenko et al. (2014); Gigoux et al. (2000); Grandia et al. (2000); Hagedorn et al. (1993); Heijlen et al. (2003); Henry bet al. (2001); Jowet et al; (1987); Kechra et al. (2003); Mertz et al. (1991); Muchez et al. (2022); Munoz et al. (2005); Navarro-Ciurana et al. (2018); Piqué et al. (2000); Ricordel et al. (2007); Schaltegger et al. (1995); Schlegel et al. (2007); Scleicher et al. (2006); Schärer et al. (1999); Schneider et al. (1999, 2003); Schott and Peres (1987a, b)Symons et al. (2009, 2011); Thiry et al. (2006); Timar-Geng et al. (2004, 2006); and Yans (2003).

Nature	Sample	Type	Size	$T_{m\ hh}$	$T_{m\ ice}$	T_h (L)	Raman salinity
				(°C)	(°C)	(°C)	wt.% eq. NaCl
Stolzembourg							
dolomite (Dol2)	ZA014	primary Lw	10-20 µm		-19.6; -20.2	90-105 (16)	
dolomite (Dol2)	ZA074	primary Lw	10-20 µm		-14/-11 (5)	130.8-142 (17)	15
dolomite (Dol2)	ZA092-1	primary Lw	10-20 µm	-25.4	-11.2	145-95 (6)	
dolomite (Dol2)	ZA092-2	p-secondary Lw	10-20 µm		-12	131.1-141 (4)	
dolomite (Dol2)	ZA031-1	primary Lw	10-20 µm		nd	139.5-146	
dolomite (Dol2)	ZA031-2	primary Lw	10-20 µm		-21.3	140-146	
dolomite (Dol2)	ZA031-3	primary Lw	10-20 µm	-37/-28 (7)	-22/-20.6 (13)	144.5-122.5 (13)	
dolomite (Dol2)	STOL1-1	primary Lw	20 µm		-15.7/-12.8 (3)		
dolomite (Dol2)	STOL2-1	primary Lw	10-20 µm	-26; -26	-20.3;-19.4	139;140	
dolomite (Dol2)	STOL4	primary Lw	10-20 µm	-33/-25 (4)	-21/-19.2 (4)	148.6-141.9 (4)	
quartz Q2	ZA031-qtz	primary Lw	5-20 µm	-43/-31 (4)	-19.6/-14.3 (13)	116.5-84.3	
quartz Q2	ZA074-qtz	primary Lw	5-20 µm	-31; -30	-23/-19.1 (5)	107.3-134.5 (5)	
quartz Q4	STOL-Qtz-4	primary Lw	5-20 µm	-31	-22/-17	108-134	
Allerborn							
quartz	ZE120	secondary Lw	10 µm		-6/-2 (3)	211-220 (277*) (5)	
sphalerite	ZE60	primary Lw	10 µm		nd	93	
Soleuvre							
barite	ZM127	primary Lw	10-20 µm		-8.5	100	
Martelange							
quartz	ZE004	secondary Lw	10 µm		metastable (1.5)	107-130 (3)	1.5

Table 1: Microthermometric data obtained on fluid inclusions from Stolzenbourg, Allerborn, Soleuvre and Martelange. Several sub-samples were studied in some samples. $T_{m\ hh}$: hydrohalite melting temperature, $T_{m\ ice}$: ice melting temperature, T_h : bulk homogenization temperature to the liquid state.

1524
1525

1526